A T-MATRIX APPROACH TO HEAVY QUARK INTERACTION WITH THERMAL GLUONS IN A QUARK GLUON PLASMA

A Thesis

by

KYLE STUART HUGGINS

Submitted to the Office of Graduate Studies of
Texas A&M University
in partial fulfillment of the requirements for the degree of

MASTER OF SCIENCE

August 2012

Major Subject: Physics

A T-MATRIX APPROACH TO HEAVY QUARK INTERACTION WITH THERMAL GLUONS IN A QUARK GLUON PLASMA

A Thesis

by

KYLE STUART HUGGINS

Submitted to the Office of Graduate Studies of
Texas A&M University
in partial fulfillment of the requirements for the degree of

MASTER OF SCIENCE

Approved by:

Chair of Committee,	Ralf Rapp
Committee Members,	Rainer Fries
	Charles M. Folden III
Head of Department,	George Welch

August 2012

Major Subject: Physics

ABSTRACT

A T-Matrix Approach to Heavy Quark Interaction with Thermal Gluons in a Quark Gluon Plasma.

(August 2012)

Kyle Stuart Huggins, B.S., Texas A&M University

Chair of Advisory Committee: Dr. Ralf Rapp

The interactions of heavy quarks within the Quark Gluon Plasma (QGP) are interpreted utilizing an elastic, thermodynamic, 2-body T-matrix in order to calculate drag coefficients of heavy-quark systems derived from a Fokker-Planck equation. A spacelike momentum constraint is employed and produces an effective, color dependent potential with the addition of relativistic factors motivated by the appropriate Feynman diagrams. Hard Thermal Loop (HTL) corrections are interpreted in the context of a finite temperature quark-gluon system, allowing a non-perturbative determination of the gluon's contribution to the drag coefficient. An enhancement of the relaxation rate of ~ 2 is observed at low momenta, leading to an enhancement of the overall relaxation rate of 20%, while the high-p limit approaches a perturbative level. The importance of a nonperturbative treatment of the QGP to reproduce the dynamical drag coefficient is illustrated.

ACKNOWLEDGMENTS

I would like to acknowledge the help and contributions of my advisor Ralf Rapp and my fellow colleagues, Felix Riek, Min He, and Paul Hohler. Their helpful discussions and open doors helped me finish my degree. I would also like to thank my wife, whose boundless patience as I finished up my degree deserves my neverending gratitude.

NOMENCLATURE

HQ	Heavy Quark
GP	Gluon Plasma
BS	Bethe Salpeter
LS	Lippmann Schwinger
QGP	Quark Gluon Plasma
QCD	Quantum Chromodynamics
lQCD	Lattice QCD
pQCD	Perturbative QCD
LO pQCD	Leading Order pQCD
npQCD	Nonperturbative QCD
RHIC	Relativistic Heavy Ion Collider
LHC	Large Hadron Collider
HTL	Hard Thermal Loop

TABLE OF CONTENTS

Page

LIST OF FIGURES

FIGURE Page

FIGURE Page

I. INTRODUCTION

A. The Quark Gluon Plasma

The formulation of a complete theory of the atomic world has been the subject of research for hundreds of years. The make up of matter has been expanded to include atoms, then electrons and protons/neutrons, and then one step farther to include quarks. Today's modern particle accelerators, such as the Relativistic Heavy Ion Collider (RHIC) at Brookhaven National Laboratories and the Large Hadron Collider (LHC) at CERN, continue to probe matter at scales never before reached, and continue to surprise scientists with sometimes revolutionary results.

One such investigation into the fundamental properties of sub-atomic particles involves exploring the (currently) innermost workings of protons and neutrons that make up the nuclei of the elements. These quarks, which are bound together by gluons, constitute the smallest division modern science has for the known particles. They combine to produce composite particles known as hadrons. Due to confinement [1], they cannot be directly observed; however, it is possible to analyze their effects on other particles by colliding nuclei together with sufficiently high energy to reach a stage where quarks become deconfined and interact more readily with the surrounding particles. This deconfined phase of matter is known as the Quark Gluon Plasma (QGP).

It is the purpose of this thesis to investigate an approach to modeling the interaction between the constituent particles in the medium by utilizing and expanding upon an established method of analysis using scattering amplitudes, or the Transition matrix. By expanding on the analytical baseline for the interaction evolution of quarks (specifically the heavy flavors c and b) I can form a more complete picture of how the QGP forms at these heavy-ion colliders and gain insight into the fundamen-

This thesis follows the style of Physical Review D.

tal properties of matter. See [2] for a review on the current state of QGP physics with heavy quarks.

This chapter is organized into two parts. First, I outline the genesis of the theoretical tools used to analyze the QGP. The next section details how the theoretical baseline is connected to the experimental results observed by colliders like LHC and RHIC.

B. Scattering theory

To fully describe the collision between two particles, one must first find some measurable quantity that can be investigated. As particles collide, they interact to produce excited states or change the physical wave function of the outbound particle. It would be meaningful to model this interaction to understand how an incoming particle might be modified by another particle. I begin by following the derivation outlined in [3]. As a particle moves, it is described as a wave packet moving through space. It will collide with some other particle and possibly scatter into a new state that is described by a new wave packet. I will call the scattering state ψ and the initial state, χ_a, where a refers to a specific incoming state. Conversely, b will refer to a specific outgoing state that I can evolve backwards in time to coincide with the same scattering state ψ. I can define an evolution operator which will move the wave packet from an initial state to a state at another time by, $U(t) = e^{-iHt}$, where H is the Hamilton operator that is divided into a free part and an interacting part, $H = H^0 + V$. Applying this operator to the interacting state, there should exist the following limits,

$$U(t)|\psi\rangle \underset{t\to-\infty}{\to} U^0(t)|\chi_a\rangle, \tag{1.1}$$

where $U^0(t)$ is defined in terms of the free Hamiltonian H^0. This implies that by taking $|\psi\rangle$ to the asymptotic past, the wave packet should be the same as the incoming wave packet, $|\chi_a\rangle$. The reverse is also true; taking some $|\psi\rangle$ to $t = +\infty$ would

yield an asymptotic state, $|\chi_b\rangle$. This is known as the asymptotic condition, and is a cornerstone for scattering theory. I rearrange the equation to express the evolved state in terms of the original,

$$|\psi\rangle \underset{t\to-\infty}{\to} U^\dagger(t)U^0(t)|\chi_a\rangle. \tag{1.2}$$

I will label the two operators generated by this formulation, $\Omega_{a,b} = \left(U^\dagger(t)U^0(t)\right)\Big|_{a,b}$ where a and b not only refer to the incoming and outgoing states, respectively, but also the limiting value of t ($-\infty$ for a and $+\infty$ for b). These are known as the Møller operators, and relate the incoming and outgoing states to the interaction state via time evolution operators. It becomes apparent then,

$$|\chi_b\rangle = \Omega_b^\dagger\Omega_a|\chi_a\rangle, \tag{1.3}$$

$$= S|\chi_a\rangle, \tag{1.4}$$

where S is the S-matrix of scattering theory. Thus the probability for an incoming state a to scatter into an outgoing state b is

$$P(a\to b) = |\langle\Omega_b\chi_b|\Omega_a|\chi_a\rangle|^2 = |\langle\chi_b|S|\chi_a\rangle|^2. \tag{1.5}$$

This is interpreted as the S corresponding to the scattering matrix component evolving the state χ_a to an asymptotic state χ_b. So S is a transition operator, encoding the information of the interaction. A typical hypothesis is that the interaction can be represented as the free particle case (no collision) and an interacting part; one can then separate the S operator into an interacting and non-interacting part loosely pictured as

$$\hat{S} \sim 1 + \hat{T}. \tag{1.6}$$

The nontrivial physics of the collision would then be constrained to the operator $\hat{T}$. The following derivation outlines how this operator is constructed.

It is possible to generate a definition of the $\hat{T}$ operator when acting on incoming and outgoing momentum states utilizing a Lippmann-Schwinger equation; the result will be central to the development of a $\hat{T}$ operator based heavy quark (HQ) diffusion model.

Consider the operator identity,

$$A^{-1} = B^{-1} + B^{-1}(B - A)A^{-1}. \tag{1.7}$$

Letting $A = z - H$ and $B = z - H^0$, where z represents complex values of energy, this can be rewritten,

$$G(z) = G^0(z) + G^0(z)VG(z), \tag{1.8}$$

where $G(z) = (z - H)^{-1}$ and $G^0(z) = (z - H^0)^{-1}$. With great malice of forethought, I construct a new operator called $T(z)$,

$$T(z) = V + VG(z)V. \tag{1.9}$$

Multiplying Eq. (1.9) by G^0, an important relation is derived,

$$\begin{aligned} G^0T &= (G^0 + G^0VG)V \\ &= GV. \end{aligned} \tag{1.10}$$

By switching the definitions of A and B, a similar expression $TG^0 = VG$ can be obtained. Plugging this result back into Eq. (1.9) will yield the operator formulation of the T-matrix,

$$T(z) = V + VG^0(z)T(z). \tag{1.11}$$

The S-matrix shall now be used to create an alternate expression written in terms of the transition matrix. First, one must write S in terms of the Møller operators,

$$\begin{aligned}\langle\chi_b|S|\chi_a\rangle &= \langle\chi_b|\Omega_b^\dagger\Omega_a|\chi_a\rangle \\ &= \lim_{\substack{t\to+\infty \\ t'\to-\infty}} \langle\chi_b|(e^{-i(H-H^0)t}e^{i(H-H^0)t'}|\chi_a\rangle.\end{aligned} \tag{1.12}$$

The order in which the limits are taken is arbitrary; for convenience there is a substitution by setting $t' = -t$ and simply taking the limit as $t \to +\infty$. A common technique used for rewriting this expression is to write it as the integral of its derivative,

$$\frac{d}{dt}[e^{iH^0t}e^{-2iHt}e^{iH^0t}] = -i(e^{iH^0t}Ve^{-2iHt}e^{iH^0t} + e^{iH^0t}e^{-2iHt}Ve^{iH^0t}), \tag{1.13}$$

where one integrates this expression and obtains the following after applying the $t \to +\infty$ limit,

$$\langle\chi_b|S|\chi_a\rangle = \langle\chi_b|\chi_a\rangle - i\int_0^\infty dt\langle\chi_b|(e^{iH^0t}Ve^{-2iHt}e^{iH^0t} + e^{iH^0t}e^{-2iHt}Ve^{iH^0t})|\chi_a\rangle. \tag{1.14}$$

Noting that the potential must be local and not act at large distances, one can equally approximate the potential as

$$V_{\text{damped}} \approx Ve^{-\eta|\tau|}, \tag{1.15}$$

where η approaches zero and τ is time. This factor only impacts the the system at large times in the past and future by damping a potential where it is already assumed to be negligible to begin with. That is, given an absolutely convergent integral,

$$\int_0^\infty d\tau|\chi_a\rangle = \lim_{\eta\to+0}\int_0^\infty d\tau e^{-\eta|\tau|}|\chi_a\rangle. \tag{1.16}$$

With this in mind, Eq. (1.14) can be reworked after replacing the proper vectors with their momentum eigenstates $|\mathbf{p}\rangle$ and $|\mathbf{p}'\rangle$,

$$\begin{aligned}\langle\mathbf{p}'|S|\mathbf{p}\rangle =&\delta^{(3)}(\mathbf{p}'-\mathbf{p}) - i\lim_{\eta\to+0}\int_0^\infty dt\langle\mathbf{p}'|(Ve^{i(E_{\mathbf{p}'}+E_{\mathbf{p}}-2H+i\eta)t} + e^{i(E_{\mathbf{p}'}+E_{\mathbf{p}}-2H+i\eta)t}V)|\mathbf{p}\rangle \\ =&\delta^{(3)}(\mathbf{p}'-\mathbf{p}) + \frac{1}{2}\lim_{\eta\to+0}\langle\mathbf{p}'|[VG(\frac{E_{\mathbf{p}'}+E_{\mathbf{p}}}{2}+i\eta) + G(\frac{E_{\mathbf{p}'}+E_{\mathbf{p}}}{2}+i\eta)V]|\mathbf{p}\rangle,\end{aligned} \tag{1.17}$$

where $G(\frac{E_{\mathbf{p}'}+E_{\mathbf{p}}}{2}+i\eta)$ is the full propagator and $E_{\mathbf{p},\mathbf{p}'}$ are the energy eigenvalues of the incoming and outgoing momentum. Utilizing the relations derived in Eq. (1.10), GV and VG are replaced with G^0T and TG^0 respectively, and the free G^0's act on their momentum eigenstates to give

$$\begin{aligned}\langle\mathbf{p}'|S|\mathbf{p}\rangle = \delta^{(3)}(\mathbf{p}'-\mathbf{p}) + \lim_{\eta\to+0}\Big[\frac{1}{E_{\mathbf{p}'}-E_{\mathbf{p}}+i\eta} + \frac{1}{E_{\mathbf{p}}-E_{\mathbf{p}'}+i\eta}\Big] \\ \times\langle\mathbf{p}'|T(\frac{E_{\mathbf{p}'}+E_{\mathbf{p}}}{2}+i\eta)|\mathbf{p}\rangle.\end{aligned} \tag{1.18}$$

The bracketed term is merely a delta function in energy, $-2\pi i\delta(E_{\mathbf{p}'}-E_{\mathbf{p}})$, simplifying the final result to

$$\langle\mathbf{p}'|S|\mathbf{p}\rangle = \delta^{(3)}(\mathbf{p}'-\mathbf{p}) - 2\pi i\delta(E_{\mathbf{p}'}-E_{\mathbf{p}})\lim_{\eta\to+0}\langle\mathbf{p}'|T(E_{\mathbf{p}}+i\eta)|\mathbf{p}\rangle. \tag{1.19}$$

This important result forms the cornerstone of scattering theory. The first term corresponds to the free particle case where no interaction occurs. The second term encodes the interaction between the two particles. Thus while the whole term rep-

resents the scattering of the particle, the second is pragmatically all that is cared about. This is the first hint that the operator $T(z)$ is representative of the physics of the system. Examining the $T(z)$ defined above in Eq. (1.9), one can apply the momentum states $|\mathbf{p}\rangle$ and $|\mathbf{p}'\rangle$,

$$\langle \mathbf{p}'|T(z)|\mathbf{p}\rangle = \langle \mathbf{p}'|V|\mathbf{p}\rangle + \langle \mathbf{p}'|VG^0T(z)|\mathbf{p}\rangle, \tag{1.20}$$

and after inserting a complete set of momentum states, $|\mathbf{k}\rangle$, it can be rewritten as

$$\langle \mathbf{p}'|T(z)|\mathbf{p}\rangle = \langle \mathbf{p}'|V|\mathbf{p}\rangle + \int d^3k \frac{\langle \mathbf{p}'|V|\mathbf{k}\rangle}{z - E_{\mathbf{k}}} \langle \mathbf{k}|T(z)|\mathbf{p}\rangle. \tag{1.21}$$

Here $\mathbf{p}$ and $\mathbf{p}'$ describe the relative incoming and outgoing momenta, V is an interacting potential and k is an intermediate momentum. This is a description of the T-matrix in a numerically approachable form. This form can also be generated by a 3D reduction of the Bethe Salpeter [4] 4D equation. It is this close connection between the Lippmann-Schwinger and Bethe-Salpeter equation that motivates the use of a potential for V [5]. If a potential can be established between two particles, a description of the interaction can be provided.

C. Importance of T-matrix

Given the current understanding of the T-matrix, one may ask how it will be applied to provide meaningful results. The most important step would be to compare it to experimental results. To that effect, one can approximate the density of a HQ in phase space as a Boltzmann equation [6] in terms of two coefficients: the drag and diffusion coefficient. The "drag" coefficient describes the average change in momentum per unit time, while the "diffusion" coefficient is the average momentum broadening per unit time. If one could describe both coefficients one could describe the phase space density of charm and bottom quarks. In Ref. [7] the T-matrix is

shown to describe the scattering amplitude that is used in the following derivation. It would be beneficial to determine the T-matrix because it not only permits a realistic (though still parameter fit) potential, it nonperturbatively resums all the ladder diagrams rather than implementing a cutoff at some order in the Born series. That is, instead of iterating Eq. (1.11),

$$T = V + VG^0V + VG^0VG^0V + \cdots , \tag{1.22}$$

I numerically solve for T by inverting the matrix element $(1 - VG^0)$.

I now reproduce part of the derivation from [6] to see how the drag coefficient will be a central part to determining the overall diffusion of a HQ in medium. Under the assumption of a uniform medium the equation of motion is governed by a semi-classical Boltzmann equation,

$$\frac{\partial}{\partial t} f(\mathbf{p}, t) = \Big(\frac{\partial f}{\partial t}\Big)_{collisions}, \tag{1.23}$$

where f is the phase space density of a heavy particle (charm or bottom). Letting $w(\mathbf{p}, \mathbf{k})$ be the rate of collisions that change the momentum of the heavy quark from $\mathbf{p}$ to $\mathbf{p} - \mathbf{k}$, Eq. (1.23) can be written as

$$\frac{\partial f}{\partial t}_{collisions} = \int d^3k (w(\mathbf{p} + \mathbf{k}, \mathbf{k}) f(\mathbf{p} + \mathbf{k}) - w(\mathbf{p}, \mathbf{k}) f(\mathbf{p})), \tag{1.24}$$

with w being the contribution to the rate from gluon, light quark and anti-light quark scattering. Here the rate is understood to be the rate due to particles knocked into a higher momentum state subtracted from its initial contribution to the rate. Thus only interactions are counted. This rate is similar to the differential cross section

derived from scattering theory; I will delve into more detail on that in later chapters. Given the cross section, the rate for just the gluons will be

$$w_g(\mathbf{p},\mathbf{k}) = \gamma_g \int \frac{d^3\mathbf{q}}{(2\pi)^3}\hat{f}(\mathbf{q})v^{q,p}\sigma_g^{p,q\to p-k,q+k}, \tag{1.25}$$

where $\gamma_g = 2\times 8$ is the degeneracy of the gluons (8 colors, 2 polarizations), $\hat{f}$ is the gluon distribution in phase space, v is the relative velocity, and σ is the differential cross section given by

$$\sigma_g = \frac{1}{(2\pi)^6 v^{q,p} 2\omega_q 2\omega_p \gamma_g \gamma_c}\sum |\mathcal{M}|^2 \frac{1}{2\omega_{k+q}2\omega_{p-k}}(2\pi)^4\delta(\omega_p+\omega_q-\omega_{p-k}-\omega_{q+k}). \tag{1.26}$$

Here ω represents the energy of the incoming/outgoing state and γ_c refers to the degeneracy of quarks. Utilizing the Landau approximation, most quark gluon scattering is assumed soft and so Eq. (1.24) is expanded in powers of $\mathbf{k}$ to obtain

$$\frac{\partial f}{\partial t} = \frac{\partial}{\partial p_i}\Big[A_i(\mathbf{p})f + \frac{\partial}{\partial p_j}[B_{ij}(\mathbf{p})f]\Big], \tag{1.27}$$

where A_i is defined by

$$A_i = \int \frac{d^3\mathbf{q}d^3\mathbf{q}'d^3\mathbf{p}'}{(2\pi)^9 2\omega_p 2\omega_q 2\omega_{q'} 2\omega_{p'}\gamma_c}\sum |\mathcal{M}|^2(2\pi)^4\delta^{(4)}(p+q-p'-q')\hat{f}(\mathbf{q})(p-p')_i. \tag{1.28}$$

In this equation, p, q, q', q' represent 4-momenta. To briefly summarize notation, 4-momenta, 3-momenta, and energy will always be denoted p_i, $\mathbf{p}_i$, and ω_i or E_i respectively. All that remains is to specify the matrix elements $\mathcal{M}$ to completely define the drag coefficient, A. As illustrated in [7], one can derive an expression for $\mathcal{M}$ in terms of the T-matrix. The question remains, why should the T-matrix formalism be used over the already defined matrix amplitudes, $\mathcal{M}$? It would be

far simpler to just use them as given and not jump through these hoops. The differentiating factor, and in fact, the motivation for this study, is that confinement in the QGP cannot be expressed in the Feynman formalism. There is no string "diagram". Additionally, the large coupling of the Coulomb term prevents accuracy of perturbative QCD (pQCD) at low energies. Treating it nonperturbatively via a 4D Bethe-Salpeter equation [4] encounters difficulties due to each particle possessing its own time coordinates. Indeed, this presents an additional challenge for performing the "straightforward" calculation via the scattering amplitude. The challenge then becomes to incorporate the phenomenologically important aspect of confinement in the machinery created for Feynman-like amplitudes. Thus the purpose of the T-matrix defined in Eq. (1.21); here is an equation for T governed by a potential V and propagator. This allows some freedom of choice regarding what form V has. Motivation for an appropriate V stems from lattice QCD (lQCD) results. Indeed, [8, 9] theorized a potential that has both string and Coulomb-like behavior for HQ scattering off light quarks; this potential model is the one I shall follow. However, the distinct element of this thesis is the incorporation of the gluon particles in the medium. In the next section, I shall recapitulate the construction of a potential capable of including both the color-Coulomb characteristics as well as confinement. In section III, I examine the finite temperature properties of the gluon vertices and any impact they might have on relativistic corrections. Section IV lays out the T-matrix formalism as it is applied to a static potential and section V contains the results of the drag coefficient calculations. I summarize and conclude in section VI.

II. CONSTRUCTING AN IN-MEDIUM POTENTIAL

A. Introduction

The ongoing issue with producing a successful model of the QGP is an appropriate choice of the theoretical underpinnings that lead to a realistic and workable portrayal of the interaction. The difficulty in proposing a model stems from the unobservable nature of quarks. The detectable quantities are largely the decay products that the detector sees and not a "quark" signature. There is thus some ambiguity in choosing an appropriate methodology. For this paper, I will build upon a method established by [10, 11] by expanding it to include the gluon interaction. The drag produced by gluons is independent of other constituent particles, so it can be determined separately. The integral form of the Lippmann-Schwinger equation suggests a solution via a potential ansatz. The potential must incorporate the non-trivial feature of confinement; this is done by utilizing thermal lQCD calculations. It is here where a fit to parameters is made. As the following discussion will be at finite temperature, T, I will rely on context to clarify when the T corresponds to the T-matrix or temperature, T. I summarize briefly how this potential is created in the next section.

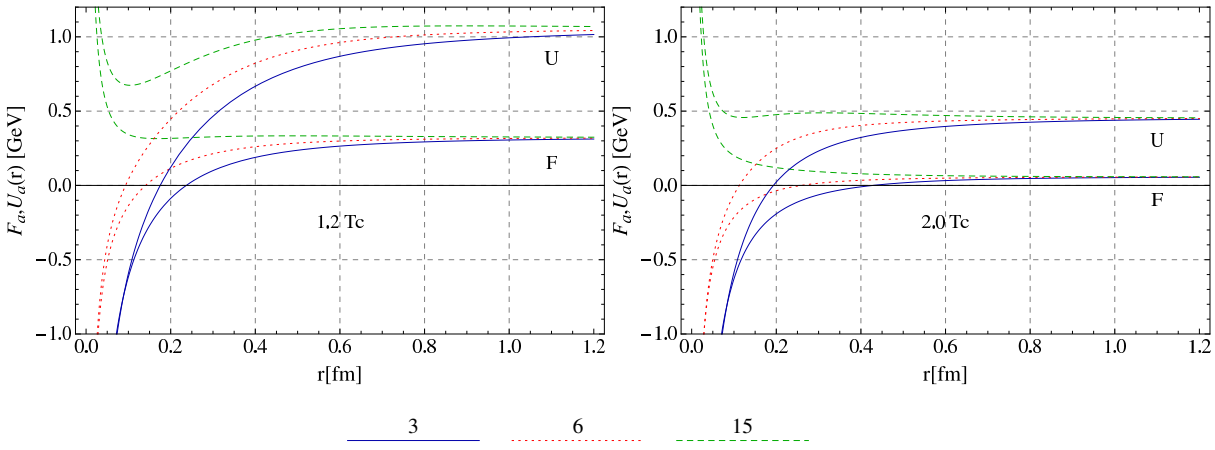

FIG. 2.1 In-medium HQ free and internal energies determined using lattice data [12] in the triplet (solid lines), sextet (dotted lines), and 15-plet (dashed lines) channels at temperatures $T = 1.2T_c$ (left) and $2T_c$ (right). Color online.

B. Static potential

Recent computations of the static HQ free energy by examining two heavy quarks separated by a distance r in thermal lQCD have revived the potential-based approach to quarkonia in the QGP. However, a functional fit to static coordinate-space is somewhat limited in flexibility and its microscopic interpretation. As in Ref. [13] I refer to the microscopic model put forward by Megias et al. [8, 9], in which the free energy in different color channels, a, is described through in-medium color-Coulomb and confining terms as

$$F_a(T,r) = -\frac{4}{3}\alpha_s\left(\frac{C_a}{r}e^{-m_D r} + \frac{m_G^2}{2\tilde{m}_D}e^{-\tilde{m}_D r} - \frac{m_G^2}{2\tilde{m}_D} + m_D\right). \tag{2.1}$$

Here it is assumed that the (remnants of the) string term (second term), as well as the long-distance-limit represented by the last two terms, are color-blind. The terms m_D, m_G, $\tilde{m}_D$, and α_s are parameters fit to the lQCD data [13] and are temperature dependent. The variable r refers to the distance separating the two particles, C_a is the Casimir factor, and α_s is the coupling factor of QCD. For the color-Coulomb

(first) term, one obtains the standard (perturbative) Casimir scaling resulting in the following coefficients for quark-antiquark, quark-quark and quark-gluon channels, respectively [14],

$$\begin{aligned} C_1 &= 1 \quad , \; C_8 = -1/8 \; , \\ C_6 &= -1/4 \; , \; C_{\bar{3}} = 1/2 \quad , \qquad (2.2) \\ C_3 &= 9/8 \quad , \; C_6 = 3/8 \quad , \; C_{15} = -3/8 \; . \qquad (2.3) \end{aligned}$$

The quark-gluon representations (bottom row) will be utilized in this thesis with the other two reproduced here for completeness. They are relevant when computing any $Q-q$ quantities. The actual fits of the four model parameters α_s, m_D, $\tilde{m}_D$ and m_G to the lQCD data [12] for the color-averaged have been performed in Ref. [13] at different temperatures, from $1.2\,T_c$ up to $\sim 2\,T_c$, where T_c refers to the critical temperature of the QGP; for the relevant lattice data [12] used in this thesis, $T_c = 196$ MeV. After determination of these quantities, the internal energy follows as

$$U(T,r) = F(T,r) - T\frac{d}{dT}F(T,r). \qquad (2.4)$$

The resulting coordinate-space potentials in the HQ-gluon color projections are summarized in Fig. 2.1.

There is currently no consensus as to whether the free or internal energy (or combinations thereof) should be used as a static potential in a Schrödinger (or Lippmann-Schwinger) equation. I will perform the calculation for both U and F. As usual, the infinite-distance limits will be subtracted to define the genuine two-body interaction contribution in each case,

$$V_a(T,r) = X_a(T,r) - X(T,\infty) \; , \; X = F \text{ or } U \; , \qquad (2.5)$$

and reinsert $X(T, \infty)$ into the calculation by interpreting it as a temperature-dependent mass term of the heavy anti-/quarks.

The baseline potentials have now been fully formed. It remains to elaborate the effects of relativistic corrections for the case at hand, i.e., HQ-gluon scattering.

III. RELATIVITY AT FINITE TEMPERATURES

A. Introduction

Forming a relativistic potential has the benefit of being valid at all energies and allows for the proper physical implementation of high energy physics. However, there is no implicit relativistic behavior in the static potential ansatz. One can implement such features by utilizing the Feynman diagrams associated with the leading order interaction to represent real potentials [15].

Special care will be given to the perturbative (Coulomb) heavy quark-gluon (Q-g) Feynman diagram at finite temperature. The hot plasma can generate Hard Thermal Loop (HTL) corrections to the vertices that, at certain momenta, can contribute at the same order in $g = \sqrt{4\pi\alpha_s}$ as the bare vertex. Additionally, there is evidence [16] that the gluon only possesses transverse degrees of freedom in computations of the high-T lattice equation of state. Typically a massive spin-1 boson will have polarizations of -1, 0, and 1. However, the longitudinal mode will be suppressed in order to meet the expected degrees of freedom.

The first section will outline the relativistic corrections to the potential terms, with specific analysis starting from the cross section. The next section will examine finite temperature effects due to HTL diagrams and calculate the corrections explicitly.

B. Relativistic corrections to potential terms

To evaluate corrections to the static potential picture, I analyze Feynman diagrams associated with the string and Coulomb terms to identify the components that might modify the existing potential. I will divide the potential into a Coulombic part, V^c, and a string part, V^s, and treat the diagrammatic corrections to each separately, similar to Ref. [13].

For the Coulombic part, I refer to the quark-gluon diagram given in Fig. 3.1 as the relevant physics of the interaction. Two separate definitions of the unique cross section will yield a relationship between the scattering amplitude, $\mathcal{M}$, and the nonrelativistic limit of the T-matrix. The two definitions follow from Bjorken-Drell [17] and Goldberger [18], respectively (normalized to $\bar{u}u = 1$),

$$d\sigma = \frac{m_1 m_3}{\omega_1 \omega_2 |\mathbf{v}_1 - \mathbf{v}_2|} \int \frac{d^3p_3}{2\omega_3 (2\pi)^3} \frac{d^3p_4}{2\omega_4 (2\pi)^3} |\mathcal{M}|^2 (2\pi)^4 \delta^{(4)}(p_3 + p_4 - p_1 - p_2) \tag{3.1}$$

$$d\sigma = \frac{1}{\omega_1 \omega_2 |\mathbf{v}_1 - \mathbf{v}_2|} \int \frac{d^3p_3}{2\omega_3 (2\pi)^3} \frac{d^3p_4}{2\omega_4 (2\pi)^3} |\sqrt{\omega_1 \omega_2} T \sqrt{2\omega_3 2\omega_4}|^2 (2\pi)^4 \delta^{(4)}(p_3 + p_4 - p_1 - p_2). \tag{3.2}$$

Here, m_i refers to the mass of the incoming/outgoing particles. These two equations identically describe a boson-fermion interaction, with the unique physics tied into a general scattering amplitude or the T-matrix. The factors of 2 applied to Eq. (3.2) within the absolute value bars have been supplied to make the connection between the two equations self-evident. Consequently,

$$\sqrt{\omega_1 \omega_2} T \sqrt{2\omega_3 2\omega_4} = \sqrt{m_1 m_3} \mathcal{M}. \tag{3.3}$$

Quoting the appendices of Herrmann [19],

$$T = \sqrt{\frac{m_1 m_2 m_3 m_4}{\omega_1 \omega_2 \omega_3 \omega_4}} \tilde{T}, \tag{3.4}$$

where T is the nonrelativistic limit of the $\tilde{T}$-matrix; the relevant quantity for this study is the latter. It is important to note that $\tilde{T}$ is fully relativistic and thus permits identifying the "corrections" necessary to make the potential ansatz relativistic as well. This gives a simple relationship between the $\tilde{T}$-matrix and the scattering amplitude $\mathcal{M}$ for fermion-boson interactions,

$$\tilde{T} = \frac{1}{2\sqrt{m_2 m_4}} \mathcal{M}. \tag{3.5}$$

In the Born approximation $\tilde{T}$ is replaced with the potential, $\tilde{V}$. This gives a general ansatz for how the static potential should behave in a fully relativistic regime,

$$\tilde{V} = \frac{1}{2\sqrt{m_2 m_4}} \mathcal{M}. \tag{3.6}$$

At this point the potential is identified by elements of the scattering amplitude $\mathcal{M}$ and a mass factor dictated by the choice of Bjorken-Drell normalization. The discussion has been general, so $\mathcal{M}$ can refer to any number of diagrams that are

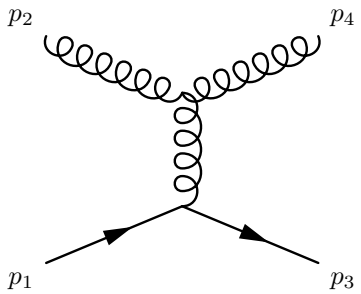

FIG. 3.1 t-channel gluon exchange for Q-g scattering. Relative incoming and outgoing 4-momentum are respectively, $q = (p_2 - p_1)/2$ and $q' = (p_4 - p_3)/2$.

included. For the arguments to follow, I now divide $\mathcal{M}$ into a Coulombic and string part,

$$\mathcal{M} = \mathcal{M}^c + \mathcal{M}^s, \tag{3.7}$$

where the Coulombic part is given diagrammatically by Fig. 3.1 and the string portion by Fig. 3.2. To identify which factors produce the relativistic corrections, I further divide $\mathcal{M}^c$ into two components, a Yukawa-like potential and a spinor dependent quantity,

$$\mathcal{M}^c = -\, i \underbrace{\frac{C_A g^2}{t - m_D^2}}_{\text{Yukawa}} \underbrace{\bar{u}(p_3)(-i\gamma^\mu)u(p_1)\epsilon(p_4)^*_\rho \Gamma^{\rho\lambda}_\mu \epsilon(p_2)_\lambda}_{\text{Spinor}}, \tag{3.8}$$

where u denotes the HQ spinors, ϵ the gluon polarization vectors, $\Gamma^{\rho\lambda}_\mu$ the 3-gluon vertex, C_A is the color factor, g is the coupling constant, γ^u are the usual Dirac gamma matrices, and $1/(t - m_D^2)$ is the gluon exchange propagator. The 3-gluon vertex is given by

$$\Gamma^{\rho\lambda}_\mu = -\,(-g^{\rho\lambda}(p_4 + p_2)_\mu + g^\lambda_\mu (p_2 - q)^\rho + g^\rho_\mu (q + p_4)^\lambda).$$

The color and coupling constants will no longer be written, as they will be contained in the definition of V^c. The Yukawa term is merely the Fourier transform of the Coulombic static potential ansatz provided in Eq. (2.1), while the second term must contain the new relativistic physics. That is,

$$\tilde{V}^c = \frac{1}{2\sqrt{m_2 m_4}} V^c| - i\bar{u}(p_3)(-i\gamma^\mu)u(p_1)\epsilon(p_4)^*_\rho \Gamma^{\rho\lambda}_\mu \epsilon(p_2)_\lambda|. \tag{3.9}$$

The spinor terms are calculated by taking the absolute value and then contracting across the vertices. This generates a relativistic definition of the Coulombic part of the static potential ansatz; an identical association is made for the string component,

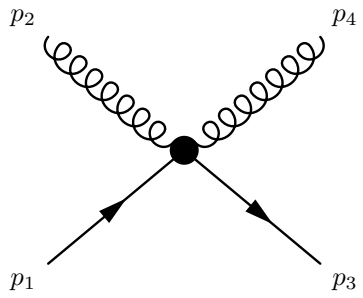

FIG. 3.2 Approximation of scalar interaction for string term.

illustrated later on by Eq. (3.36). But before this is done, the finite temperature effects on the vertices must be dealt with, specifically an analysis on any Hard Thermal Loop (HTL) corrections.

C. Finite temperature corrections

One concern is that at finite temperature the Feynman diagram will necessarily be modified. There will be additional diagrams which make an easy analysis problematic. It would thus be beneficial to include finite temperature corrections in a gauge-invariant way. I treat this by referring to the HTL approximation to anticipate the higher order contributions to the 3-gluon vertex at finite T. The fundamental physics behind HTLs was elaborated by Braaten and Pisarski in two papers, [20,21]. Hard Thermal Loops are calculated based on the assumption that the internal momentum is large compared to external momenta. Using the nomenclature of Eq. (3.10), this implies $k \gg p$. For the 3-gluon vertex, there are contributions from a gluon loop, ghost loop and quark loop (Figs. 3.3(a)-(c)). Diagram 3.3(d) has one power less in exchange momentum, so it does not contribute to the HTL approximation. The gluon contribution (Fig. 3.3(a)) reads

$$\Gamma^{(gl)}(p_1, p_2, p_3) = ig^3 C_a f_{abc} \int \frac{d^4k}{4\pi} 9 k_\mu k_\nu k_\rho \Delta(k)\Delta(p_2 - k)\Delta(p_3 + k), \qquad (3.10)$$

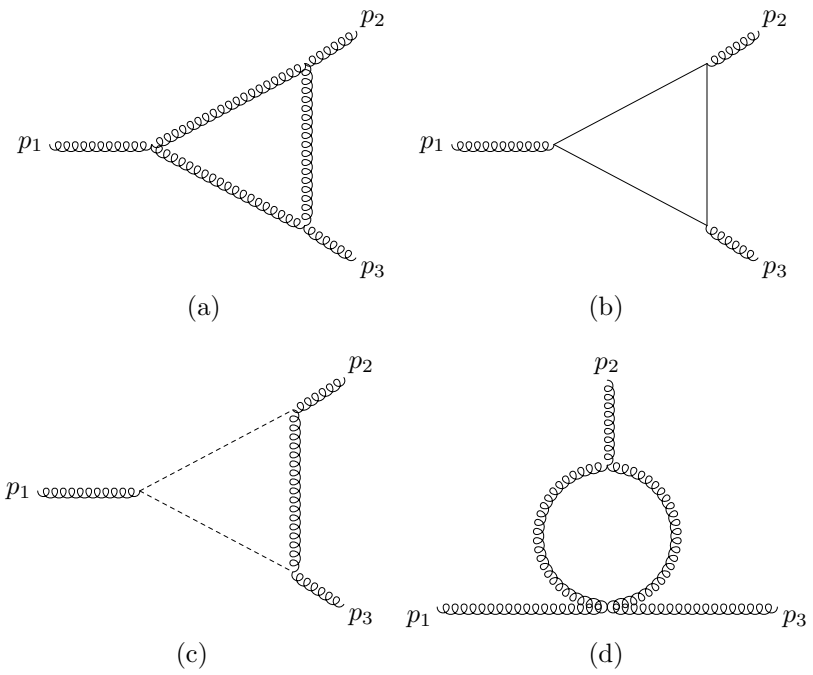

FIG. 3.3 3-gluon vertex corrections. Solid lines are quarks while dashed are ghosts.

where p_i is the 4-momentum of the external lines, g is the coupling constant, C_a and f_{abc} are color factors, and k is the exchanged momentum between p_2 and p_3. The deltas represent gluon propagators.

I can examine how the contribution will behave in T by utilizing general power counting arguments [20]. Disregarding the powers of k in the numerator for a moment, the propagator contributions will schematically integrate to

$$\int \frac{d^4k}{(2\pi)^4}\Delta(k)\Delta(p_2-k)\Delta(p_3+k) \propto \int \frac{dk}{kp}X, \tag{3.11}$$

where X depends on the statistics of the interacting particles. There are three possible cases: (i) X involves a sum of statistical factors of the same kind (both Fermi or both Bose), (ii) X is a difference of statistical factors of the same kind, and (iii) X is a difference of statistical factors of different kinds. Case (i) and (ii)

could occur for the 3-gluon vertex, while (iii) occurs for the quark-gluon vertex. However, case (i) will cancel out because it is associated with the $T = 0$ divergence and the 3-gluon vertex is only linearly divergent. Examining the 3-gluon vertex (ii), it schematically integrates to $X \propto \frac{dn}{dk} \to 1/T$. Combining the above equation with the kinematic contributions of the vertex, the gluon HTL correction will behave as

$$g^3 \int \frac{dk}{kp} k^3 X \propto g^3 T^2 p^{-1}. \tag{3.12}$$

So if $p \approx gT$, then the HTL correction is of order g^2T, which is the same as the zeroth order 3-gluon vertex. However, in the regime I am concerned with, the gluons' momenta are of the same order as the heat bath and thus $p \approx T$. Then the 3-gluon vertex will be of order $\sim g^3T$ while the vertex is $\sim gT$, rending the HTL correction subleading. It is then sufficient to use the bare vertex at finite temperature. A similar argument is carried out for the quark-gluon vertex and other 3-gluon loop corrections in Fig. 3.3.

To determine the effects of including the diagrammatic components in the potential, I calculate $\tilde{V}^c$ by utilizing the standard completeness relations that sum over spin (s) and polarization states (r), respectively,

$$\sum_s u_\mu(p,s)\bar{u}_\nu(p,s) = \Big(\frac{\not{p} + m}{2m}\Big)_{\mu\nu}, \tag{3.13}$$

$$\sum_r \epsilon^*_\mu(p,r)\epsilon_\nu(p,r) = g_{\mu\nu} - \frac{p_\mu p_\nu}{m^2}. \tag{3.14}$$

Evaluating the spinor terms of Eq. (3.8) by first replacing the u's with the completeness relation from Eqs. (3.13,3.14) yields

$$\begin{aligned}\Pi = &|\bar{u}(p_3)\gamma^\mu u(p_1)\epsilon(p_4)^*_\rho \Gamma^{\rho\lambda}_\mu \epsilon(p_2)_\lambda|^2 \\ =&\frac{\mathrm{Tr}\{(\not{p}_3 + m_1)\gamma^\mu(\not{p}_1 + m_1)\gamma^\sigma\}}{4m_1^2}\times \\ &\times \Gamma^{\rho\lambda}_\mu \Gamma^{\alpha\beta}_\sigma E_{\alpha\beta}E_{\rho\lambda},\end{aligned} \tag{3.15}$$

where Γ and E are defined as

$$\begin{aligned}\Gamma^{\rho\lambda}_\mu =& -(-g^{\rho\lambda}(p_4+p_2)_\mu + g^\lambda_\mu(p_2-q)^\rho \\ &+ g^\rho_\mu(q+p_4)^\lambda),\end{aligned} \tag{3.16}$$

$$E_{\mu\nu} = g_{\mu\nu} - \frac{p_\mu p_\nu}{m_2^2}. \tag{3.17}$$

Examining the contraction across the Γ's and term being traced over using FeynCalc [22], I employ Mandelstam relations to simplify the result,

$$s = (p_1+p_2)^2 \to p_1\cdot p_2 = \frac{1}{2}(s - p_1^2 - p_2^2), \tag{3.18}$$

$$t = (p_1-p_3)^2 \to p_1\cdot p_3 = -\frac{1}{2}(t - p_1^2 - p_3^2), \tag{3.19}$$

$$u = (p_1-p_4)^2 \to p_1\cdot p_4 = \frac{1}{2}(-s - t + m_1^2 + m_2^2 + m_3^2 + m_4^2 - p_1^2 - p_4^2), \tag{3.20}$$

where for the last line I have used $s+t+u = m_1^2+m_2^2+m_3^2+m_4^2$. Furthermore, I employ the condition that $p^2 = m^2$. Where possible, I drop terms of order t or higher since these terms are subleading at large $s = E^2$. I now have an expression with ~ 200 terms that must be contracted with the remaining boson completeness relation. An important difference for the thermal gluon is that it does not exhibit the 3 degrees of freedom expected from theory; the longitudinally polarized gluon is

not observed as a D.o.F. To encode this characteristic, I project out the transverse modes and proceed with only those components. I use a projection operator,

$$(P_T + P_L)_{\mu\nu} = g_{\mu\nu} - \frac{p_\nu p_\mu}{m^2}, \tag{3.21}$$

$$(P_T)_{ij} = \delta_{ij} - \frac{p_i p_j}{m^2}, \tag{3.22}$$

$$(P_T)_{00} = (P_T)_{0i} = (P_T)_{j0} = 0, \tag{3.23}$$

where $i = 1, 2, 3$. Selecting only P_T, I proceed with the contraction that schematically is viewed as

$$\Pi_T = \Lambda^{ijkl}(P_T)_{ij}(P_T)_{kl} = \Lambda^{ijkl}E_{ij}E_{kl}, \tag{3.24}$$

with Λ representing the result of the first contraction. All that is left is a series of purely 3D scalar products. I use the same Mandelstam relations from Eq. (3.18-3.20) but write them in terms of their 3D scalar products,

$$\mathbf{p}_1 \cdot \mathbf{p}_2 = \frac{1}{2}(-s + m_1^2 + m_2^2 + 2\omega_1\omega_2), \tag{3.25}$$

$$\mathbf{p}_1 \cdot \mathbf{p}_3 = -\frac{1}{2}(t - m_1^2 - m_3^2 + 2\omega_1\omega_3), \tag{3.26}$$

$$\mathbf{p}_1 \cdot \mathbf{p}_4 = \frac{1}{2}(-s - t + m_2^2 + m_3^2 + 2\omega_1\omega_4), \tag{3.27}$$

where $E_i = \omega_i = \sqrt{m_i^2 + \mathbf{k}_i^2}$. Moving to the center of mass of an elastic collision sets $\omega_{1/2} = \omega_{3/4}$ and $\mathbf{p}_{1/3} = -\mathbf{p}_{2/4}$. In terms of the relative incoming momentum then, $\mathbf{q} = \mathbf{p}_1$. Then the complicated term Π_T reduces to a tractable expression,

$$\begin{aligned}\Pi_T = & \\ & \frac{2}{m_1^2}\Big((-\mathbf{q}^2(m_1-\omega_1)(m_1+\omega_1)({m_2}^2+{m_1}^2-s+2\omega_1\omega_2)^2 \\ & +({m_2}^2-{\omega_2}^2)^2({m_2}^2+{m_1}^2-s)^2+2\mathbf{q}^8)\frac{1}{\mathbf{q}^4} \\ & -4\omega_1\omega_2({m_2}^2+{m_1}^2-s)-2({m_1}^2-{\omega_1}^2)^2-4{\omega_1}^2{\omega_2}^2\Big),\end{aligned}$$

which can be simplified to the following expression, after averaging over spin states,

$$\Pi_T = \frac{1}{m_1^2}(s-m_2^2-m_1^2)^2. \tag{3.28}$$

I take Π_T as the result of the spinor structure calculation and neglect the longitudinal mode. Additionally one can set $m_{2/4} = m_g$ and $m_{1/3} = m_Q$. Referring back to Eq. (3.9), the modified potential $\tilde{V}^c$ reads

$$\tilde{V}^c = V^c\sqrt{\frac{(s-m_g^2-m_Q^2)^2}{4m_g^2m_Q^2}}. \tag{3.29}$$

The term under the square root yields the same corrections given by [13]; I adopt their convention to define the relativistic (off-shell) corrections,

$$R(q,q') = m(q)^{-1/2}m(q')^{-1/2}, \tag{3.30}$$

$$B(q,q') = b(q)^{1/2}b(q')^{1/2}, \tag{3.31}$$

$$b(q) = (1+\frac{q^2}{\omega_g(q)\omega_Q(q)}), \tag{3.32}$$

$$m(q) = \frac{m_Qm_g}{\omega_Q(q)\omega_g(q)}. \tag{3.33}$$

The fully relativistic Coulombic potential now reads

$$\tilde{V}^c = V^c R(q,q')B(q,q'). \tag{3.34}$$

This completes the relativistic correction to the Coulombic portion of the quark gluon potential. It has, in fact, yielded the same results as for the HQ-light quark calculation in the limit of small t. The string term must now be determined. To perform the same analysis on the string portion of the potential requires an ansatz of the string Lagrangian,

$$\mathcal{L} = m_g \tilde{G} A^\mu A_\mu \bar{Q} Q, \tag{3.35}$$

in a scalar approximation of the interaction. Here, $\tilde{G}$ is related to the Fourier transform of the spatial potential ansatz, $\tilde{G} \sim m_G^2/(\mathbf{q}^2 + \tilde{m}_D^2)^2$. In a similar manner as the Coulomb part, the string interaction behaves as a potential as well,

$$\tilde{V}^s = \frac{V^s}{2m_g} |\bar{u}(p_3)u(p_1)2m_g g^{\mu\nu}\epsilon(p_4)^*_\mu \epsilon(p_2)_\nu|. \tag{3.36}$$

Calculating the spinor terms yields

$$\begin{aligned}
\Xi =& |\bar{u}(p_3)u(p_1)2m_g g^{\mu\nu}\epsilon(p_4)^*_\mu \epsilon(p_2)_\nu|^2 \\
\Xi_T =& \mathrm{Tr}\{(\not{p}_1 + m_1)(\not{p}_3 + m_3)\} E_{ij} E^{ij} \frac{4m_g^2}{4m_Q^2} \\
=& (8m_Q^2 - 2t)(1 + \frac{(\mathbf{p}_2 \cdot \mathbf{p}_4)^2}{\mathbf{p}_2^2 \mathbf{p}_4^2}) \frac{4m_g^2}{4m_Q^2}.
\end{aligned} \tag{3.37}$$

Simplifying Eq. (3.19) through the elastic condition to $t = -(\mathbf{p}_2 - \mathbf{p}_4)^2$, it is plugged into Eq. (3.37),

$$\Xi_T = 8m_g^2(1 + \frac{1}{4}\frac{\mathbf{p}_2^4 + \mathbf{p}_4^4 + 2\mathbf{p}_2^2\mathbf{p}_4^2}{\mathbf{p}_2^2\mathbf{p}_4^2}). \tag{3.38}$$

An elastic collision in the center of mass implies $\mathbf{p}_2^2 = \mathbf{p}_4^2$, so Eq. (3.38) is reduced to $\Xi_T = 16m_g^2$. Averaging over spin states and plugging this all back into Eq. (3.36),

$$\tilde{V}_s = V_s \frac{\sqrt{\Xi_T/4}}{2m_g} = V_s. \tag{3.39}$$

The net result is that the string term has no relativistic correction. In order to simulate the running of α_s a logarithmic function is appended to the potential, F_{run},

$$\mathrm{F}_{run}(q,q') = \ln[\frac{\Delta^2}{\Lambda^2}]/\ln[\frac{(q-q')^2+\Delta^2}{\Lambda^2}], \tag{3.40}$$

where $\Delta = 1$ GeV and $\Lambda = 0.2$ GeV. This accounts for off-shell running coupling; the on-shell coupling is effectively dealt with by the parametrization of the spatial potential given by lQCD. With the appropriate parametrization in place, the relativistic static potential reads

$$\tilde{V}(q,q') = R(q,q')B(q,q')F_{run}(q,q')V^c(q,q') + V^s(q,q'). \tag{3.41}$$

The final step to complete the potential formulation is to expand it in partial waves. Including the color dependence, the potential input into the $\tilde{T}$-Matrix is

$$\tilde{V}_{l,a}(q,q') = R(q,q')B(q,q')F_{run}(q,q')V^c_{l,a}(q,q') + V^s_l(q,q'), \tag{3.42}$$

where $l = 0, 1, 2...$ is the partial wave channel and a is the color. With the addition of the relativistic corrections represented by R and B and the running of the coupling simulated with F_{run}, we have produced a minimally relativistic, lattice-fit potential model. This result is used as input into the $\tilde{T}$-matrix equation.

IV. T-MATRIX

A. Formalism

I now utilize the constructed potentials in a $\tilde{T}$-matrix framework. By employing the $\tilde{T}$-matrix as a 3D reduced Bethe-Salpeter equation [23–25] in the ladder approximation, a $\tilde{T}$-matrix equation is derived. A partial wave expansion yields a 1D equation which is numerically tractable,

$$\begin{aligned}\tilde{T}_{l,a}(E;q',q) =&\tilde{V}_{l,a}(q',q) + \frac{2}{\pi}\int_0^\infty dk k^2 \tilde{V}_{l,a}(q',k) \\ &\times G_{12}(E;k)\tilde{T}_{l,a}(E;k,q)[1 \pm n_1(\omega_1(k)) \pm n_2(\omega_2(k))],\end{aligned} \tag{4.1}$$

where $l = 0, 1, 2\ldots$ are the partial waves, $n_{1,2}$ correspond to thermal distribution functions for the intermediate states, and the $\pm$ signify the statistics of the particle: either boson(+) or fermion($-$). I define $q = |\mathbf{q}|$ and $q' = |\mathbf{q}'|$ as the relative 3-momenta of the incoming and outgoing states; $k = |\mathbf{k}|$ is the relative momentum of the intermediate states.

To complete the analysis of the $\tilde{T}$-matrix, the two-particle propagator G_{gQ} must be specified. It depends on the scheme of the underlying BS equation, where for this thesis I focus on the Thompson scheme,

$$G_{gQ}(q) = \frac{m(q)}{E - \omega_g(q) - \omega_Q(q) - \Sigma_g - \Sigma_Q}, \tag{4.2}$$

where $\omega_{g/Q}(q) = \sqrt{q^2 + m_{g/Q}^2}$. This choice is motivated by noting that it has been previously suggested [26] that, for the case at hand, the Thompson scheme provides a better description of vacuum spectroscopy than, say, the Blankenbecler-Sugar (BbS) equation. The masses of the heavy and light particles are determined by correcting

the bare mass; the HQ mass is dependent on the infinite distance limit of the free or internal energy,

$$m_Q = m_Q^0 + \Sigma_Q^R(T) \ , \ \Sigma_Q^R(T) = X(T,\infty)/2, \tag{4.3}$$

with $X = F$ or U. The gluon's mass is modified by including a perturbative thermal mass correction [27],

$$m_g = \sqrt{m_{g,0}^2 + m_{th}^2},$$

$$m_{g,0} = 0, \tag{4.4}$$

$$m_{th}^2 = \frac{g^2T^2}{2}(\frac{N_c}{3} + \frac{N_f}{6}). \tag{4.5}$$

I choose 3 active light flavors, and with $N_c = 3$, the thermal mass correction is $m_g = \sqrt{3/4}gT$. The choice of $N_f = 3$ is dictated by the initial lattice fit; the motivation is that these gluon contributions are planned to be included in the context of other flavors in the medium. So while this study is performed with emphasis on gluons, it will later be incorporated with the up, down, and strange flavors to paint a broader picture of how a heavy quark diffuses in the QGP.

It remains to specify the bare masses of the heavy quarks. The effective masses are provided by a fit to vacuum spectroscopy; for this choice of potential the parameters are $m_c^0 = 1.264$ GeV and $m_b^0 = 4.662$ GeV. In medium, for both charm and bottom sectors, the combined particle width is fixed at 200 MeV, giving a self energy to each particle of 50 MeV. That is,

$$\Gamma_{g,Q} = -2\mathrm{Im}\Sigma_{g,Q}, \qquad \mathrm{Im}\Sigma_{g,Q} = -50 \text{ MeV}. \tag{4.6}$$

In principle, this self energy depends self consistently on the $\tilde{T}$-matrix. However, previous studies [28] indicate that the self-consistent evaluation of the self energy

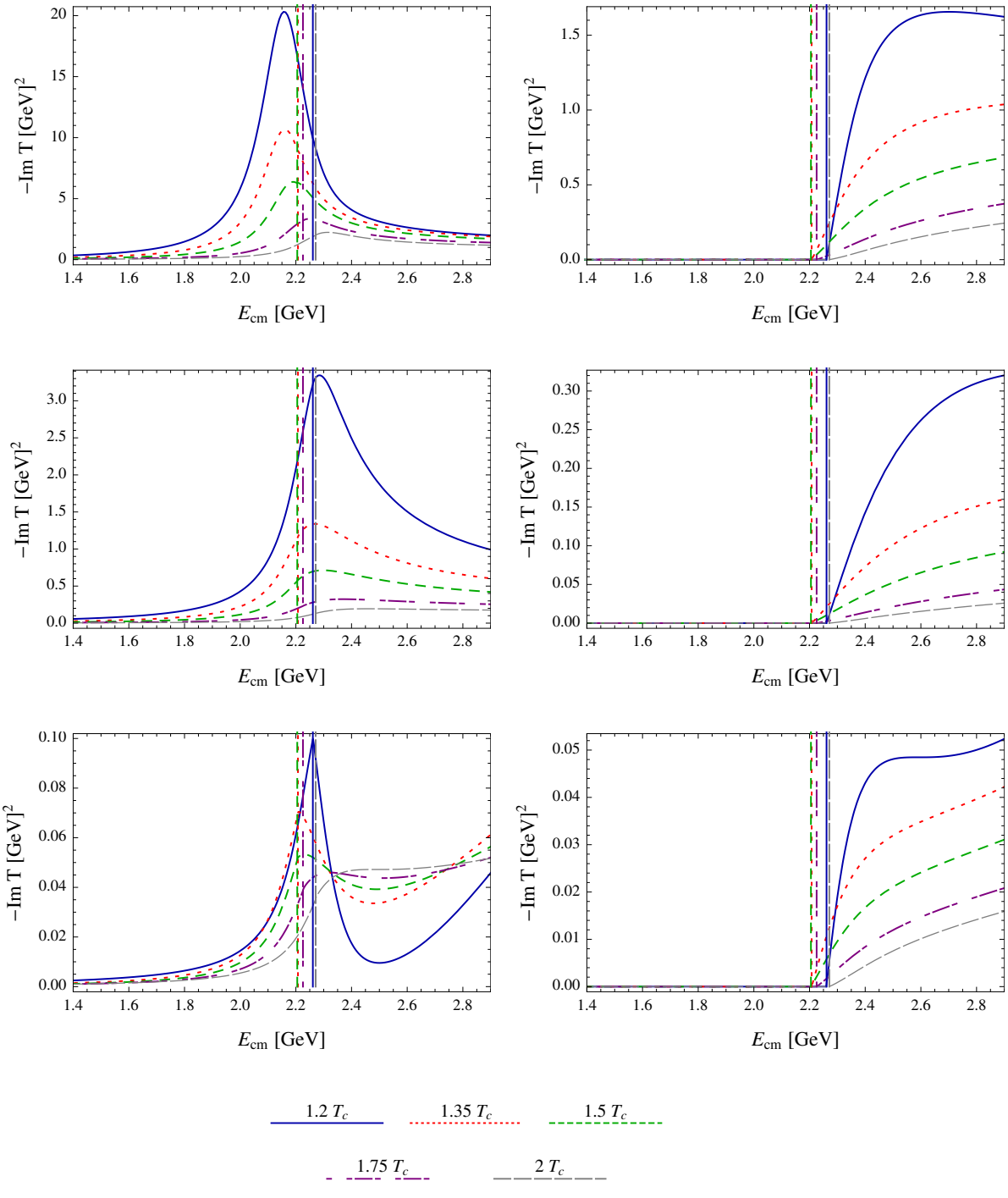

FIG. 4.1 Imaginary part of the on-shell charm-gluon for s-wave (left) and p-wave (right) $\tilde{T}$-matrix for the triplet (upper), sextet (middle), and 15-plet (bottom) channels using U as a potential and a fixed two-particle width of 200 MeV. Vertical lines correspond to the energy threshold of the given temperature. Color online.

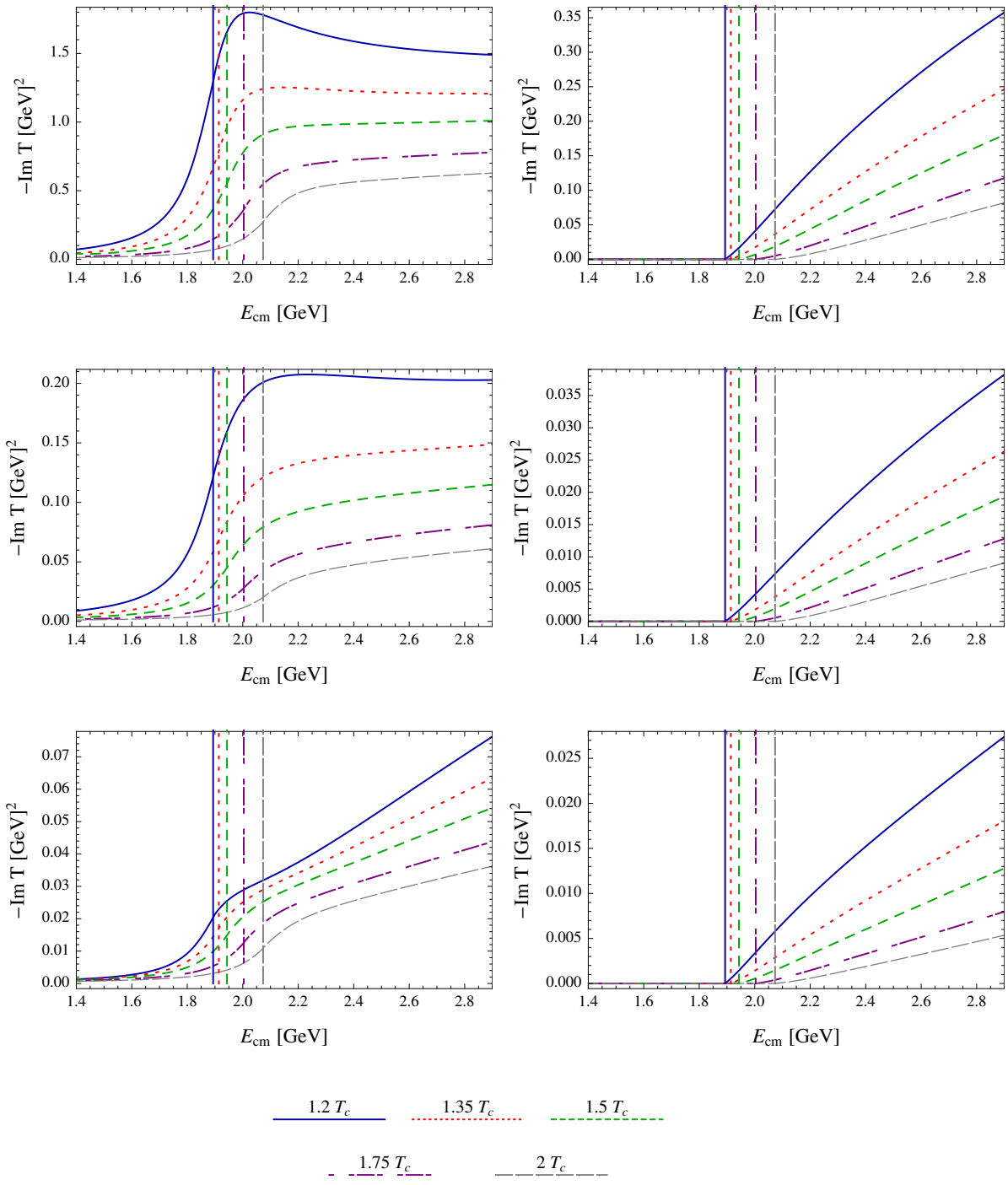

FIG. 4.2 Imaginary part of the on-shell charm-gluon for s-wave (left) and p-wave (right) $\tilde{T}$-matrix for the triplet (upper), sextet (middle), and 15-plet (bottom) channels using F as a potential and a fixed two-particle width of 200 MeV.

will produce a $\tilde{T}$-matrix not very different to the fixed value approximation lending justification to its use.

Plotted in Fig. 4.1 and 4.2 are the imaginary parts of the $\tilde{T}$ matrix, with vertical lines corresponding to the threshold energy $(m_g + m_Q)$ for internal and free energies, respectively. Examining the results of the $\tilde{T}$-matrix calculations, Fig. 4.1 indicates that a resonance-like enhancement persists in the triplet channel up to $1.5T_c$, while it melts earlier in the sextet channel. The 15-plet produces a very shallow resonance as suggested by the spatial potential in Fig. 2.1. The results indicate suppression in the sextet and 15-plet by factors of 5 and 200, respectively, when compared to the triplet channel. P-wave contributions are around 20% of the s-wave strength. Changing the input potential to the free energy F (Fig. 4.2) moves the threshold below the enhancement in the S-wave and the attractive resonance structure universally disappears in all channels for all temperatures, excluding perhaps the triplet at $1.2T_c$. In addition, the threshold energy values continually increase as opposed to the non-monotonic behavior of the internal energy's threshold value. This is attributed to the dominance of the thermal mass contribution of the gluon over the free energy infinite distance limit given to the HQ's mass.

B. Coulomb only behavior

To further investigate the behavior of the different components of the potential ansatz, I perform identical calculations using the Coulomb portion, $\tilde{V}_c$, of the potential only. The nonperturbative term is set to zero and the potential is purely Coulombic. Two competing effects appear; the infinite distance mass correction becomes smaller (and possibly negative 2.1). The mass modification enhances the potential through the relativistic corrections (Eq. (3.30)) and loss of confinement suppresses (enhances) attractive (repulsive) potentials. This is borne out in Fig. 4.3 by noting the suppression in the triplet($\sim 1/2$) and sextet($\sim 1/5$) channels relative to the full potential, while the 15-plet increases by a factor of $\sim$4. In fact,

the enhancement structure of the 15-plet in Fig. 4.1 is mitigated in the Coulomb, disappearing much more quickly for higher T. However, overall the 15-plet gains an enhanced repulsive rescattering strength since the string term is attractive in nature. The sextet presents the strongest effect due to the Coulomb already being suppressed by the Casimir factor; the nonperturbative term plays the strongest role here. Another important component is the threshold energy. In the full potential at 1.2 T_c the threshold is at $\sim$ 2.3 GeV, while in the Coulomb it is at $\sim$ 1.7 GeV. This increases the size of the phase space by pushing the interaction strength above threshold (compare the vertical lines in Fig. 4.1 and 4.3 for instance), allowing for more possible interactions when the HQ propagates in the medium. Additionally, the Coulomb $\tilde{T}$-matrix peaks much closer to threshold in the triplet, enhancing the interaction above threshold. These kinematic effects cloud up the distinction between the two cases, lending naive expectations of the Coulomb result unadvisable. In the Coulomb, threshold enhancement is universally absent in the p-wave.

It is important to note that the $\tilde{T}$-matrix to be used in the next section is modified by an additional mass-dependent term (Eq. (3.4)) which will affect its overall behavior. As will be shown, however, at low momentum the lack of nonperturbative physics will still be apparent in the drag coefficient.

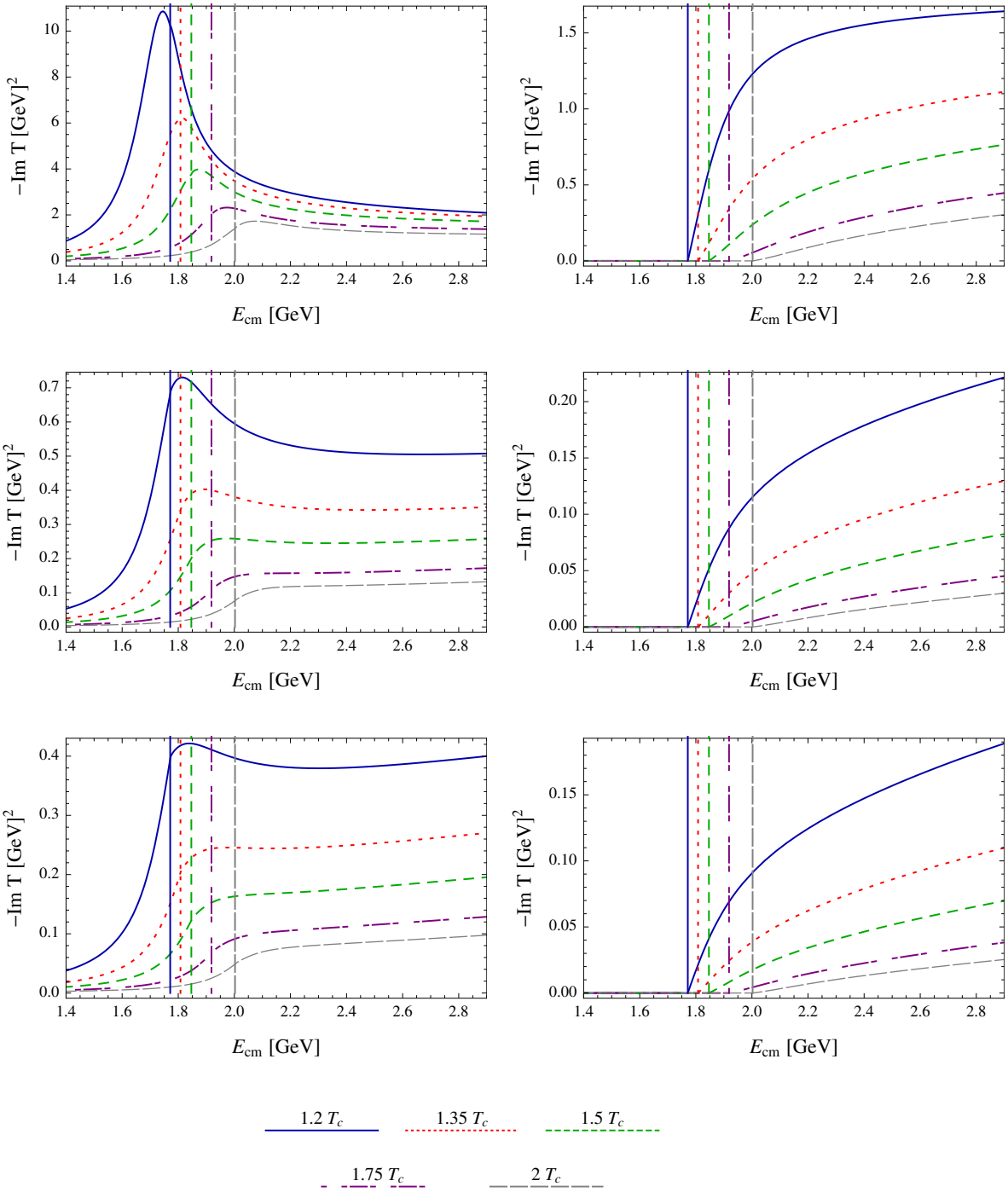

FIG. 4.3 Same as Fig. 4.1, but for Coulomb only potential.

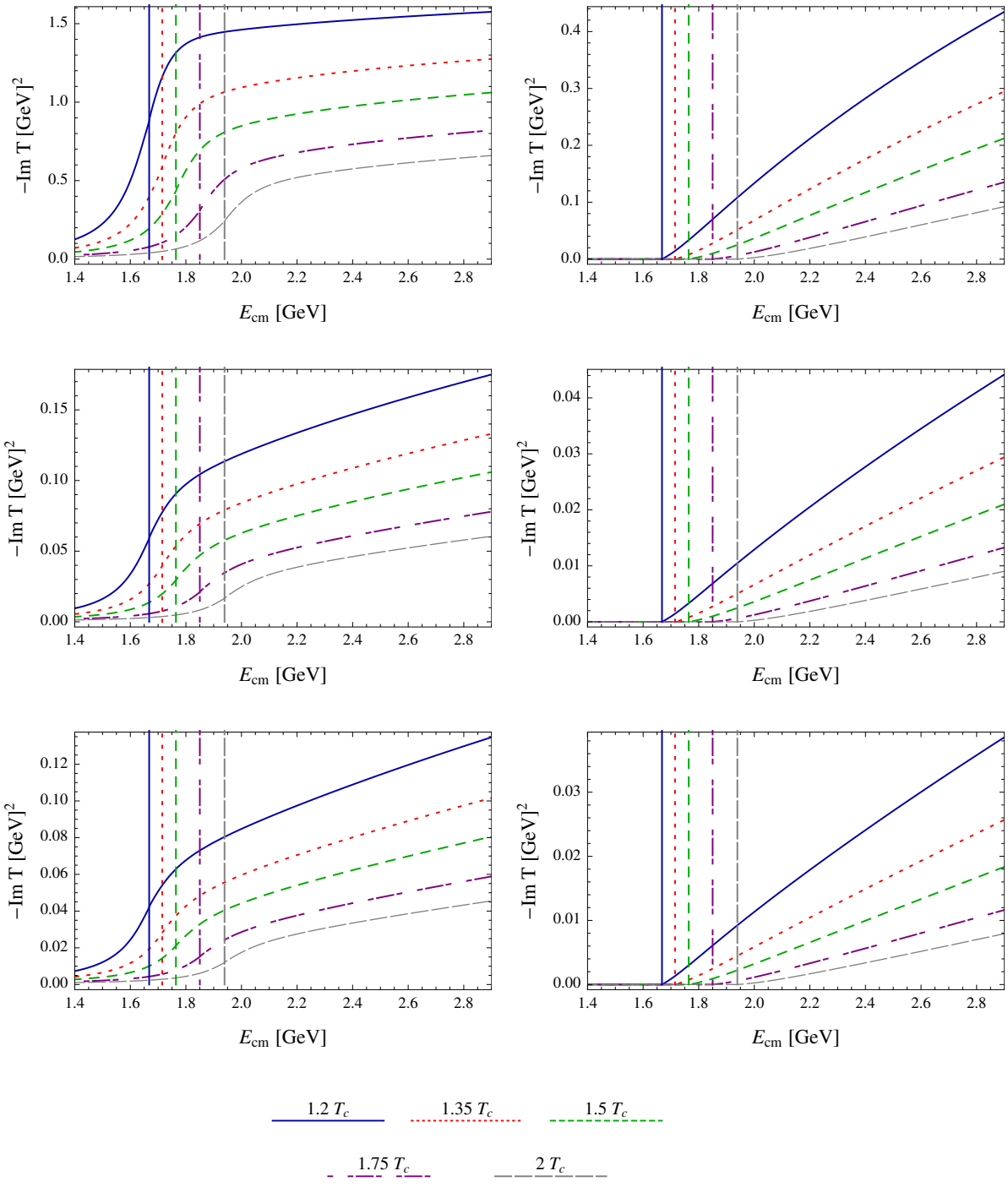

FIG. 4.4 Same as Fig. 4.2, but for Coulomb only potential.

V. TRANSPORT COEFFICIENT

A. Heavy quark diffusion

I now turn to the diffusion properties of a single heavy quark in the context of a heavy quark-gluon (Q-g) $\tilde{T}$-matrix. As outlined in section I, the Boltzmann equation is approximated by a Fokker-Planck equation to determine the relaxation rate,

$$\gamma_Q = 1/\tau_Q \equiv \lim_{p\to 0} A(\mathbf{p}), \tag{5.1}$$

with the drag coefficient for Q-g scattering,

$$\begin{aligned} A(\mathbf{p}) =& \frac{1}{16(2\pi)^9\omega_Q(p)} \int \frac{d^3q}{\omega_g(q)} n_F(\omega_g(q)) \int \frac{d^3q'}{\omega_g(q')} \\ & \times \int \frac{d^3p'}{\omega_Q(p')} \frac{(2\pi)^4}{d_c} \sum |\mathcal{M}|^2 \delta^{(4)}(q+p-q'-p')(1-\frac{\mathbf{p}\cdot\mathbf{p}'}{\mathbf{p}^2}). \end{aligned} \tag{5.2}$$

The scattering amplitude is given by a partial wave expansion, summed and averaged over initial and final color states,

$$\begin{aligned} \sum |\mathcal{M}|^2 =& \frac{64\pi}{s^2}(s-m_g^2+m_Q^2)^2(s-m_Q^2+m_g^2)^2 \\ & \times \sum_a d_a(|T_{a,0}(s)|^2 + 3|T_{a,1}(s)\cos\theta_{cm}|^2), \end{aligned} \tag{5.3}$$

where $T_{a,i}$ is the nonrelativistic T-matrix defined in Eq. (3.2), related to $\tilde{T}_{a,i}$ (the scattering matrix described by Eq. (4.1)) by Eq. (3.4),

$$T_{a,i}(s) = m(p_{cm})^{1/2} \tilde{T}_{a,i}(E; p_{cm}, p_{cm}) m(p_{cm})^{1/2}, \tag{5.4}$$

$$E = \sqrt{s} = \omega_g(p_{cm}) + \omega_Q(p_{cm}), \tag{5.5}$$

$$p_{cm} = \frac{1}{2E}\sqrt{m_Q^4 + (m_g^2-s)^2 - 2m_Q^2(m_g^2+s)}, \tag{5.6}$$

with color degeneracies of

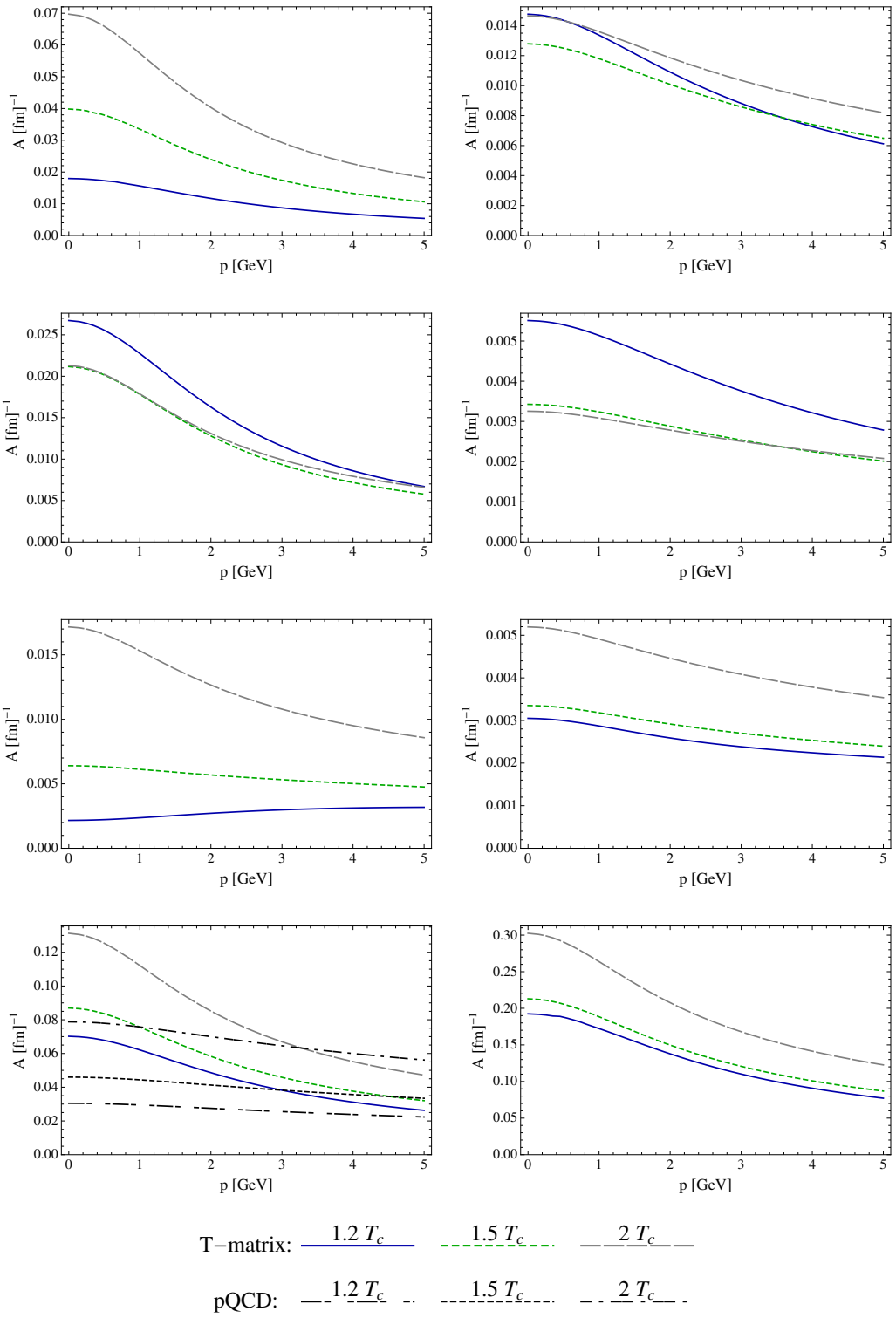

FIG. 5.1 Drag coefficients in the s-wave (left) and p-wave (right) from charm-gluon $\tilde{T}$-matrix interactions using potential U for the triplet (top), sextet (2nd row), and 15-plet (3rd row) color channels. Their sums are given for the gluon only (bottom left) and gluon, light, and strange particles (bottom right) as determined by [13].

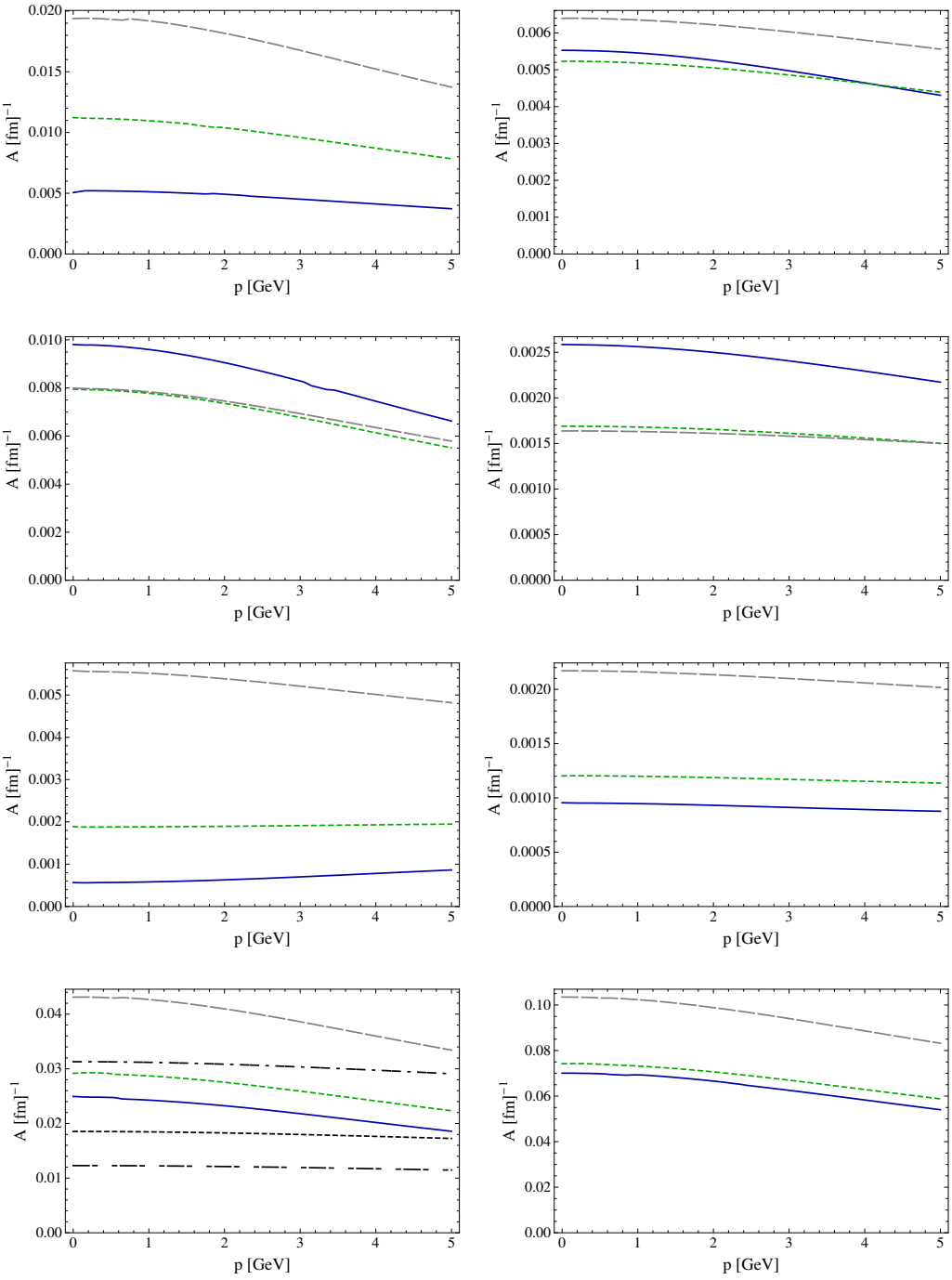

FIG. 5.2 Same as Fig. 5.1, but for bottom quarks.

$$\begin{aligned} \text{Fermions: } & d_0 = 1, \quad d_{\bar{3}} = 3, \quad d_6 = 6, \quad d_8 = 8, \\ \text{Bosons: } & d_3 = 3, \quad d_6 = 6, \quad d_{15} = 15. \end{aligned} \tag{5.7}$$

The drag coefficient in Eq. (5.2) is applied individually for the light, strange, and gluon sector. The light sector is doubly degenerate with an up and down quark while there is only one strange particle. With the determination of the gluon $\tilde{T}$-matrix, I can now produce an explicit determination of its contribution to the drag coefficient in the context of all the light quarks in medium, represented by the bottom right graph in Fig. 5.1, 5.2.

Examining the results of the nonperturbative $\tilde{T}$-matrix calculations in the context of the drag coefficient at $1.2T_c$ reveals that the sextet channel produces a stronger drag coefficient ($\gamma_c = 0.027$ fm^{-1}) as compared to the triplet channel ($\gamma_c = 0.018$ fm^{-1}), whose Casimir factor would indicate the reverse should be true; however, while the triplet channel does have a larger color Coulomb factor, the degeneracy insures the sextet channel has a stronger total coefficient since the sextet degeneracy is larger. The $\tilde{T}$-matrix indicates that the triplet does produce a larger bound state, but note that the drag coefficient only integrates over energies above threshold. The 15-plet gains little ground due to its degeneracy; its contribution remains quite small. The bottom left plot in Fig. 5.1 compares the Q-g result to leading order pQCD (LO pQCD) with a coupling constant of $\alpha_s = 0.4$. Summing over all channels gives a relaxation rate of $\gamma_c = 0.07$ fm^{-1} at $1.2T_c$. This is a factor 2.3 times larger than the pQCD estimate. Note that at $1.2T_c$ the pQCD and $\tilde{T}$-matrix results converge at high p. However, at $2T_c$, it appears pQCD overestimates the drag coefficient at high p and underestimates at low p. This is attributed to the coupling instituted in LO pQCD using a rather large value ($\alpha_s = 0.4$ compared to 0.3 in the lQCD potential) and the dominance of the perturbative potential at high energies. The bottom quark relaxation rate is a factor 2 larger than the pQCD estimate (0.025 vs. 0.012 fm^{-1}). The combined Q-g relaxation rate in Fig. 5.2 is $\gamma_c = 0.025$ (0.043) fm^{-1} at 1.2 (2)

T_c. The same qualitative analysis holds for the bottom quark as well as the p-wave contributions for both heavy quarks.

I also examine the drag coefficient computed from utilizing the Coulomb-only potential. Here, the behavior of the drag coefficient contribution varies depending on which channel is calculated; in the s-wave, there is enhancement in the Coulomb-only over the full potential in the triplet and 15-plet interaction, with suppression in the sextet. The relaxation rate in the Coulomb-only charm-gluon using U as a potential (Fig. 5.3) increases $\sim 40\%$ from 0.07 to 0.1 at $1.2T_c$ and only increases $\sim 15\%$ at $2T_c$; the nonperturbative effect dies towards higher temperatures as it approaches the perturbative limit. It is the interplay between color channels that ultimately determine the behavior of the drag coefficient. At $1.2T_c$, the large relative enhancement of the 15-plet (factor of 12) in the Coulomb s-wave is partially offset by the increased suppression of the sextet (factor of 0.5). In the free energy charm-gluon Coulomb-only (Fig. 5.4) the enhancement is noticeably smaller, coinciding with the interpretation of F being a more perturbative potential than U. However, the enhancement still persists. The differences in the drag coefficient between the two scenarios begin to disappear as higher momenta are reached. This is interpreted by saying that the more relativistic the particles become, the more dominant the Coulombic potential becomes since the particles are being driven closer and closer together. Thus, the nonperturbative effect dies out at high energies, exactly as expected. What is unexpected is the strength of the 15-plet in both Fig. 5.3 and 5.4; at $1.2T_c$ it is stronger than the sextet in the Coulomb approximation and has roughly the same value as the sextet full potential calculation. This is attributed to two properties: enhancement due to loss of nonperturbative effects (i.e., no cancellation between the Coulomb and string) and the mass correction dynamics; the smaller effective mass for the Coulomb-only accelerates thermalization rate. Only at increasing momentum and temperature do the two values approach each other, and even cross, as illustrated the last plot in Fig. 5.3. Nonperturbative effects thus act to reduce drag at lower

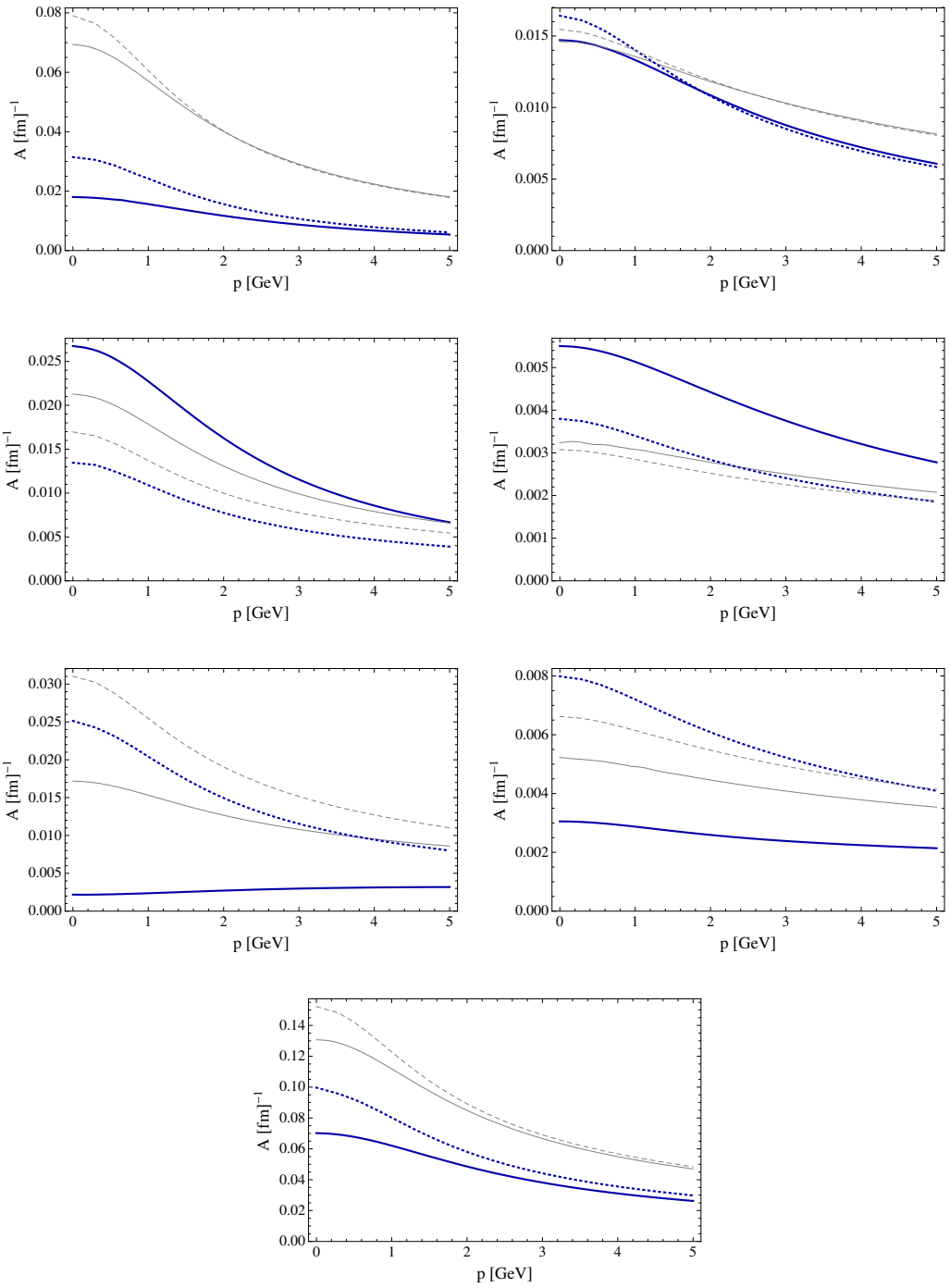

FIG. 5.3 Coulomb-only drag coefficients (dashed lines) compared to full potential (solid lines) for charm-gluon at $1.2T_c$ (thick) and $2.0T_c$ (thin). Diagrams illustrate the s-wave (left) and p-wave (right) for charm-gluon in potential U for the triplet (top), sextet (2nd row), and 15-plet (3rd row) color channels. The bottom diagram corresponds to the sum of all channels.

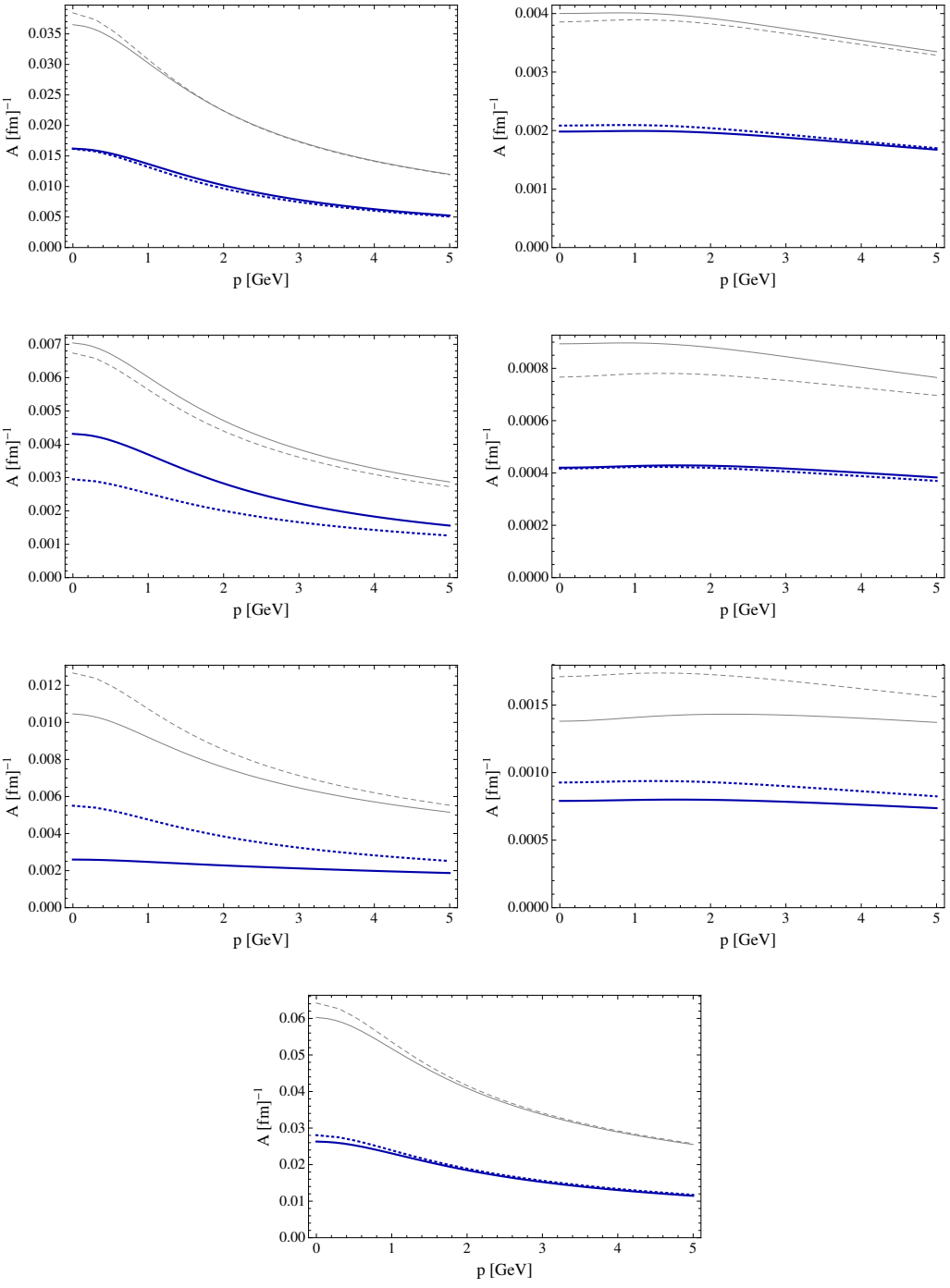

FIG. 5.4 Same as Fig. 5.3, but using F as the potential.

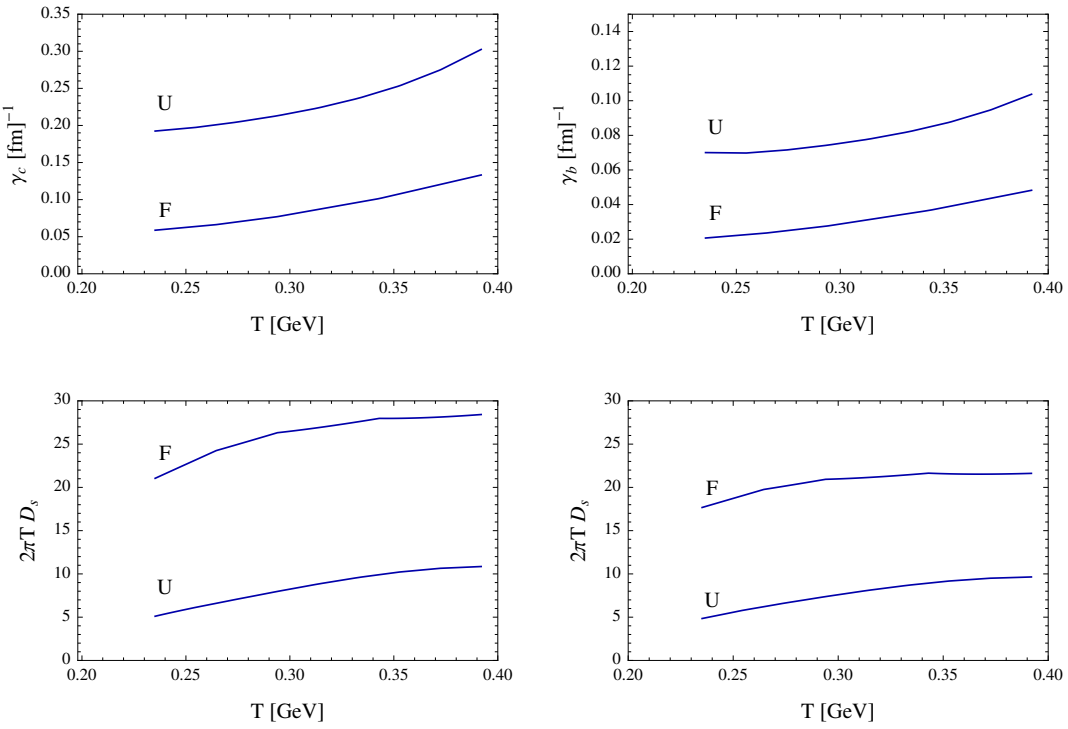

FIG. 5.5 Charm (left) and bottom (right) relaxation rates and diffusion constants using U and F as a potential.

energies. In the free energy case (Fig. 5.4) the effect is similar though much less pronounced, lending credence to verifying F as being more perturbative.

For the top plots in Fig. 5.5, the charm (bottom) - light quark as well as strange contributions are combined with the gluon rates to generate drag coefficients for the entire QGP. To this effect, a relaxation rate was obtained of $\gamma_c = 0.19$ fm^{-1} at $1.2T_c$ for the charm quark and $\gamma_b = 0.07$ fm^{-1} for the bottom quark using U as a potential; this represents a 20% increase on previous results using only pQCD Q-g interactions.

The relaxation rates can be rewritten in terms of the spatial diffusion coefficients by

$$D_s = \frac{T}{m_Q \gamma_Q}. \tag{5.8}$$

Note that this quantity essentially divides out the "kinematic" delay of the relaxation rate for a massive particle. Thus, in first approximation one may expect D_s to be independent of the HQ mass. This is one of the main reasons why this quantity, after scaling by temperature to a dimensionless quantity, has been used as an indicator of a general transport parameter of the QCD medium, namely the ratio of viscosity to entropy-density, $\eta/s \simeq cTD_s$. The coefficient c typically ranges from 1/5 to 1/2 in weakly and strongly coupled plasmas, respectively. In Fig. 5.5 I summarize the temperature dependence of γ_Q (upper panels) and D_s (lower panels) from the calculations for charm (left panels) and bottom quarks (right panels), using both free and internal energies for the input potentials. For the relaxation rate, the expected mass scaling by a factor of m_c/m_b when going from charm to bottom is roughly found, for both F and U potentials. For charm quarks the difference between the potentials translates into a factor of 4(2) increase in the relaxation rate at low (high) temperatures. This is somewhat slightly less pronounced for bottom. The anticipated independence of D_s on mass holds well for the U potential (within ca. 10%), while for the F potential the deviations are somewhat larger (ca. 20-25%). If TD_s is indeed proportional to η/s, all results are suggestive for a shallow minimum toward the critical temperature, which is nontrivial since it implies a marked increase in interaction strength with decreasing temperature. Numerically, the newly included nonperturbative treatment for HQ-gluon scattering reduced D_s by about 20% relative to the previous results [13]; for the U-potential both charm and bottom give $TD_s \simeq 0.8$ at the lowest temperature, which would imply $\eta/s \simeq 0.16 - 0.4$.

VI. CONCLUSION

A. Summary

As a model for the microscopic interactions of the QGP, I examined a nonperturbative contribution of gluons interacting with a HQ probe. This HQ provides a means to probe the QGP and thus modeling it more accurately will produce a clearer understanding of the formation of a plasma at RHIC and LHC. To overcome the challenges of describing an interaction between a HQ and a gluon, I utilized a lattice fit QCD potential with relativistic corrections. These corrections were evaluated in the context of massive bosons and finite temperature and were found to yield the same results as Q-q interactions. The HTL contributions were suppressed compared to the bare vertex. I then utilized established methods to produce a drag coefficient describing the Q-g propagation in a hot medium via the $\tilde{T}$-matrix determined using a 3D reduced BS equation. Due to ambiguities in the definition of a true potential, the drag coefficient was determined in two limiting cases which are assumed to provide the upper and lower bounds, employing the free (F) and internal (U) energies. The Q-g drag coefficient was added to previous Q-q contributions to yield an overall value of the total drag due to up, down, strange, and gluon particles.

By analyzing a gluon plasma, I have shown that its contribution produces a significant nonperturbative effect with momentum dependence and temperature dependence similar to Q-q contributions. The gluon relaxation rate γ_c is enhanced by a factor of $2-3$ when compared to the perturbative estimate in both charm and bottom cases at low momenta. Thus the gluon interaction cannot be treated perturbatively when computing total drag coefficient in the QGP. Additionally, I illustrated how confinement serves to suppress drag at low momentum and close to threshold, thus exemplifying how color neutral objects form via Q-q interactions more readily than Q-g ones.

To improve on this analysis, one could revisit the fits to lQCD made by [13] to extend them above $2T_c$ and below $1.2T_c$. It could be beneficial to confirm via direct calculation that by dropping subleading terms of order t in the relativistic corrections to the potentials the relevant physics is still described. A possible extension would be to include radiative interactions and coupled channels. Further research should clarify the proper choice of potential, whether it be U or F or some combination of the two.

By providing a complete picture of the interactions that occur in the QGP between a HQ propagating in the medium, one can understand how it will diffuse and impact the production of open and hidden-flavor hadrons at freezeout. This will generate a more complete picture of particles generated in heavy-ion collisions, putting the physics community one step closer to identifying the fundamental physics taking place not only in colliders around the world, but at the heart of the early universe.

REFERENCES

[1] K. G. Wilson, Phys. Rev. D **10**, 2445 (1974).

[2] R. Rapp, H. van Hees, in R. C. Hwa and X.-N. Wang (Ed.), *Quark Gluon Plasma 4,* (World Scientific, Hackensack, NJ, 2010), p. 111.

[3] J. Taylor, *Scattering Theory: The Quantum Theory of Nonrelativistic Collisions*, (Dover Publications, New York, NY, 2006).

[4] E. E. Salpeter and H. A. Bethe, Phys. Rev. **84**, 1232 (1951).

[5] K. Nakayama and W. G. Love, Phys. Rev. C **38**, 51 (1988).

[6] B. Svetitsky, Phys. Rev. D **37**, 2484 (1988).

[7] H. van Hees, M. Mannarelli, V. Greco, and R. Rapp, Phys. Rev. Lett. **100**, 192301 (2008).

[8] E. Megias, E. Ruiz Arriola, and L. Salcedo, JHEP **0601**, 073 (2006).

[9] E. Megias, E. Ruiz Arriola, and L. Salcedo, Phys. Rev. D **75**, 105019 (2007).

[10] D. Cabrera and R. Rapp, Phys. Rev. D **76**, 114506 (2007).

[11] M. Mannarelli and R. Rapp, Phys. Rev. C **72**, 064905 (2005).

[12] O. Kaczmarek, PoS **CPOD07**, 043 (2007).

[13] F. Riek and R. Rapp, Phys. Rev. C **82**, 035201 (2010).

[14] E. V. Shuryak and I. Zahed, Phys. Rev. D **70**, 054507 (2004).

[15] R. Machleidt, K. Holinde, and C. Elster, Physics Reports **149**, 1 (1987).

[16] P. Lévai and U. Heinz, Phys. Rev. C **57**, 1879 (1998).

[17] J. Bjorken and S. Drell, *Relativistic Quantum Mechanics*, (McGraw-Hill, New York, NY, 1964).

[18] M. Goldberger and K. Watson, *Collision Theory*, (Dover Publications, New York, NY, 2004).

[19] V. Herrmann and K. Nakayama, Phys. Rev. C **46**, 2199 (1992).

[20] E. Braaten and R. D. Pisarski, Nuclear Physics B **337**, 569 (1990).

[21] E. Braaten and R. D. Pisarski, Nuclear Physics B **339**, 310 (1990).

[22] R. Mertig, M. Böhm, and A. Denner, Computer Physics Communications **64**, 345 (1991).

[23] R. Blankenbecler and R. Sugar, Phys. Rev. **142**, 1051 (1966).

[24] R. Thompson, Phys. Rev. D **1**, 110 (1970).

[25] R. Machleidt, Adv. Nucl. Phys. **19**, 189 (1989).

[26] R. Woloshyn and A. Jackson, Nucl. Phys. B **64**, 269 (1973).

[27] M. Bellac, *Thermal Field Theory*, (Cambridge University Press, Cambridge, UK, 2000).

[28] F. Riek and R. Rapp, New J. Phys. **13**, 045007 (2011).

APPENDIX A

SCATTERING CROSS SECTION

In this appendix I will explore how the cross section is formed for fermion-boson scattering to illustrate the connection of the cross section to the scattering amplitude. The fermion-boson scattering diagram can be used to construct a cross section that corresponds to a physical observable of a system. The cross section determines the likelihood of an interaction between two particles, and is vital in calculating the total scattering of a particle in a medium. As such, I reproduce part of a derivation of the scattering cross section for fermion-boson systems in terms of the scattering amplitude, $\mathcal{M}$ which can be derived from Feynman diagrams.

First, note that the scattering amplitude for quark-gluon scattering can be written [17] (neglecting the nonscattering term) as

$$S_{fi} = -\frac{1}{V^2}\sqrt{\frac{m_1 m_3}{\omega_1(2\omega_2)\omega_3(2\omega_4)}}(2\pi)^4\delta^{(4)}(p_3 + p_4 - p_1 - p_2)\mathcal{M}. \tag{A.1}$$

S_{fi} is the scattering amplitude from an initial state to a final state and $\mathcal{M}$ is the invariant amplitude defined by a corresponding scattering diagram. The volume element V comes from normalizing the plane waves to unit probability in a box of volume V. To find the cross section, the S_{fi} amplitude is squared and divided by $V\tau$ where τ is the time interval over which the system propagates. This is a transition

probability per unit spacetime. Examining the square of the delta functions, their integral representation can be reduced,

$$[(2\pi)^4\delta^{(4)}(p_f - p_i)]^2 = (2\pi)^8\delta^{(4)}(p_f - p_i)\int_{-\tau/2}^{\tau/2} dt e^{-it(\omega_f-\omega_i)}\int_V d^3x e^{-ix(\mathbf{p}_f-\mathbf{p}_i)}$$
$$= (2\pi)^4\delta^{(4)}(p_f - p_i)V\tau. \tag{A.2}$$

Thus the probability to transition from one state to another per unit spacetime is given by

$$\mathcal{W} = \frac{|S_{fi}|^2}{V\tau} = \frac{m_1 m_3(2\pi)^4\delta^{(4)}(p_3 + p_4 - p_1 - p_2)}{V^4\omega_1(2\omega_2)\omega_3(2\omega_4)}|\mathcal{M}|^2. \tag{A.3}$$

To get the scattering cross section, one must multiply by the number of final states and divide by the flux, given by,

$$\#\text{ of particles} = V\int\frac{d^3p_3}{(2\pi)^3}V\int\frac{d^3p_4}{(2\pi)^3} \tag{A.4}$$

$$\text{flux} = \frac{|\mathbf{v}_1 - \mathbf{v}_2|}{V^2}. \tag{A.5}$$

Since I normalized to one particle per unit volume, I do not get the 2ω typical of other normalization schemes. This provides all the ingredients necessary to assemble the cross section. Note that all units of volume drop out, as expected;

$$\begin{aligned} d\sigma &= \mathcal{W} \times \frac{\#\text{ of final states}}{\text{flux}} \\ &= \frac{m_1 m_3}{\omega_1 \omega_2 |\mathbf{v}_1 - \mathbf{v}_2|} \int \frac{d^3 p_3}{2\omega_3 (2\pi)^3} \int \frac{d^3 p_4}{2\omega_4 (2\pi)^3} (2\pi)^4 \delta^{(4)}(p_3 + p_4 - p_1 - p_2) |\mathcal{M}|^2. \end{aligned} \tag{A.6}$$

This provides the cross section for fermi-boson interaction in terms of its invariant scattering amplitude. Since the derivation has been completely general, any number of $2 \to 2$ diagrams may be included in the interaction; all of the normalization factors are general for the fermion-boson case. Indeed, the expression will be identical for fermion-fermion and boson-boson scattering, with a differing normalization factor: for boson-boson collisions, replace each m/ω with $1/2\omega$ and vice versa for fermion-fermion case.

VITA

Kyle Stuart Huggins

Department of Physics and Astronomy, Cyclotron Institute tel: (+1) 979 845 1411

3366 TAMU khuggins@comp.tamu.edu

College Station, Texas 77843

EDUCATION

Texas A&M University 08.2010-

M.S. in Physics: *in progress*

Texas A&M University 08.2006-06.2010

B.S. in Physics

Minor Mathematics